Geologica Acta, Vol.11, Nº 4, December 2013, 443-463
DOI: 10.1344/105.000002059
Available online at www.geologica-acta.com

geologica acta

Geochemical and geochronological constraints on the geologic evolution of the western Sonobari Complex, northwestern México

R. VEGA-GRANILLO [1] **J.R. VIDAL-SOLANO** [1] **L. SOLARI** [2] **M. LÓPEZ-MARTÍNEZ** [3]

O.S. GÓMEZ-JUÁREZ [4] **S. HERRERA-URBINA** [1]

[1] **Departamento de Geología, Universidad de Sonora**
Rosales y Encinas S/N, Hermosillo, Sonora, México 83000 Vega-Granillo E-mail: rvega@ciencias.uson.mx

[2] **UNAM, Centro de Geociencias, Campus Juriquilla**
76001, Juriquilla, Querétaro

[3] **Departamento de Geología, Centro de Investigación Científica y de Educación Superior de Ensenada (CICESE)**
Carretera Ensenada-Tijuana nº 3918, 22860 Ensenada, Baja California, México

[4] **Unidad Académica de Ciencias de la Tierra, Universidad Autónoma de Guerrero**
Taxco el Viejo, Guerrero, México C.P 40323

ABSTRACT

In the southern Sierra Sonobari, NW México, U-Pb and $^{40}Ar/^{39}Ar$ geochronology studies allowed to define the provenance and maximum depositional age of the Francisco Gneiss basement of the Sonobari terrane and to establish the age of some magmatic events in that area. The youngest zircon cluster in paragneisses of the Francisco Gneiss indicates a maximum depositional age of 509 ± 29Ma. The main peaks of the relative probability plot yield ages of 1690 and 1404Ma with minor peaks at 1156, 921, and 517Ma. Major peaks suggest that the main source of sediments was the Paleo- and Mesoproterozoic crust of Laurentia. Orthogneiss from the Francisco Gneiss yields a U-Pb zircon upper intercept age of 248 ± 28Ma, which is interpreted as the crystallization age. Crosscutting dykes of metabasite yield an $^{40}Ar/^{39}Ar$ age of 67 ± 5Ma, which is interpreted as indicating cooling after either a latest Early Cretaceous orogenic event or Late Cretaceous contact metamorphism. Granodiorite intruding the Francisco Gneiss yields a U-Pb age of 64 ± 1Ma, which is interpreted as a magmatic age. The hornblende-plagioclase Macochin Gabbro yields $^{40}Ar/^{39}Ar$ isochron ages of 54 ± 10Ma and 47 ± 5Ma, which are interpreted as cooling ages after the gabbro intrusion. Geochemical data indicate that the mafic rocks of the Francisco Gneiss correspond to subalkaline basalts of tholeiitic affinity with concentrations of high field strength elements similar to oceanic basalts, suggesting an asthenospheric upper mantle source. However, according to the variation in Th/Yb and U/Yb, the amphibolites display a significant influence of the upper continental crust. The Macochin Gabbro also has a geochemical signature characteristic of subalkaline basalt with tholeiitic affinity, and high field strength elements similar to oceanic basalts. Tectonic discrimination diagrams and elemental distribution suggest that the mafic rocks of both the Francisco Gneiss and Macochin Gabbro were emplaced during rifting in a back-arc setting.

KEYWORDS | **Sonobari. Geochronology. Sediment provenance. Geochemistry.**

INTRODUCTION

Rocks with orogenic metamorphism play a crucial role in the understanding of the tectonic evolution of mountain chains. Because of the complexity of these rocks their study requires a multidisciplinary approach involving petrology, geocronology and geochemistry. Isolated exposures of metamorphic rocks in northern Sinaloa, northwestern México (Fig. 1A) have been regarded as the internal zones of a late Paleozoic orogen produced by the collision of Gondwanan blocks against the southern limit of Laurentia (Peiffer-Rangin, 1979; Poole *et al*., 2005). The metamorphic rocks were originally grouped in the Sonobari Complex (de Cserna and Kent, 1961), which is considered to be the basement of the Sonobari terrane of Campa and Coney (1983). Later, this terrane was included in the Tahué terrane of Sedlock *et al*. (1993). These metamorphic rocks are also included in the El Fuerte block, which consists of Gondwanan terranes accreted to southern Laurentia in the late Paleozoic (Poole *et al*., 2005). Geological relationships and extension of the Sonobari terrane or the El Fuerte block have not been defined with precision because they are mostly covered by Cenozoic volcanic and sedimentary units (Mullan, 1978). The region was affected by a Late Jurassic (?) orogenic event (Mullan, 1978; Vega-Granillo *et al*., 2011). The Alisitos arc, considered part of the Guerrero superterrane, was accreted about the latest Early Cretaceous time (*e.g*. Alsleben *et al*., 2008).

A detailed geological study of the El Fuerte region was carried out by Mullan (1978), who recognized and named the main units and assigned tentative ages based on lithological correlations. Previous works (Mullan, 1978; Keppie *et al*., 2006; Vega-Granillo *et al*., 2008, 2011) allowed the metamorphic-igneous units of this region to be separated into two distinctive suites exposed to the east and west of the town of El Fuerte (Fig. 1A). The eastern suite includes the Middle to Upper Ordovician Río Fuerte Formation, in greenschist to amphibolite facies, with low P metamorphism, whose protolith has peri-Gondwanan provenance (Vega-Granillo *et al*., 2008, 2011). This unit is intruded both by the Lower Silurian Realito Gabbro and the Upper Jurassic Cubampo Granite and covered by the Upper Jurassic volcanosedimentary Topaco Formation, all of which underwent greenschist facies metamorphism and deformation during a Late Jurassic (?) event (Mullan, 1978; Vega-Granillo *et al*., 2008, 2011, 2012). All these units are structurally overlain by the Upper Cretaceous Guamuchil Formation, a volcanic unit, which underwent greenschist facies contact metamorphism after its tectonic juxtaposition (Vega-Granillo *et al*., 2012). This work focuses on the western suite exposed in the southern Sierra Sonobari and isolated inliers along the Gulf of California coast. Metamorphic rocks of this region are included in the Francisco Gneiss, which is made of paragneiss, orthogneiss, and amphibolite. The main aims of this paper are: i) to establish the provenance and maximum deposition age of the sedimentary protoliths; ii) to determine the age of the igneous felsic protoliths; iii) to constrain the age of the metamorphic events; and iv) to find out the ages of felsic and mafic bodies intruding the metamorphic rocks. U-Pb and Ar-Ar geochronological studies were performed on selected rocks of the Francisco Gneiss and intruding igneous rocks in order to resolve these points. This work also includes a geochemical study of the mafic rocks of the Francisco Gneiss and the intruding gabbro in order to obtain an accurate classification, a basis for comparison, and to define the tectonic setting of emplacement of these rocks. The data obtained should help to constrain the geological relationships of different units and events within this orogen and to define its role in the evolution of northwestern México.

GEOLOGICAL SETTING

Three metamorphic and igneous units crop out in southern Sierra Sonobari: the Francisco Gneiss, the Macochin Intrusion (Mullan, 1978; Mullan and Bussell, 1977; Keppie *et al*., 2006), and a felsic intrusion that we name the Los Parajes Granodiorite (Fig. 1C). The Francisco Gneiss is described as banded felsic and mafic gneisses with some pelitic gneiss, affected by pervasive migmatization (Mullan, 1978). A U-Pb concordant age of ~220Ma is reported by Anderson and Schmidt (1983, data repository) and a ~206Ma age is reported by Keppie *et al*. (2006); these dates were considered to represent the age of the gneiss igneous protolith. Numerous undated foliated leucocratic dikes transect the gneisses.

Keepie *et al*. (2006) reported concordant U-Pb titanite ages from the gneisses, which range from 112 to 98Ma and are partially concordant to U-Pb xenotime ages ranging from 91 to 51Ma (Keppie *et al*., 2006). These ages are interpreted as partial resetting after a high-grade metamorphic event of imprecise age. $^{40}Ar/^{39}Ar$ analyses of gneisses yielded plateau cooling ages of 16.5 ± 1Ma (muscovite) and 13 ± 1Ma (biotite), which are interpreted as Miocene exhumation along a metamorphic core complex (Keppie *et al*., 2006); although, no detailed structural study exists to define the shear zone associated with the proposed core complex.

The Macochin Intrusion is described as a large lopolith consisting of cumulate pargasite hornblendite overlain by plagioclase-hornblende gabbro and cut by gabbroic dikes (Mullan and Bussell, 1977; Mullan, 1978). The contact between the Macochin Intrusion and the Francisco Gneiss has been considered either intrusive (Mullan, 1978) or structural (Keppie *et al*., 2006). Both the

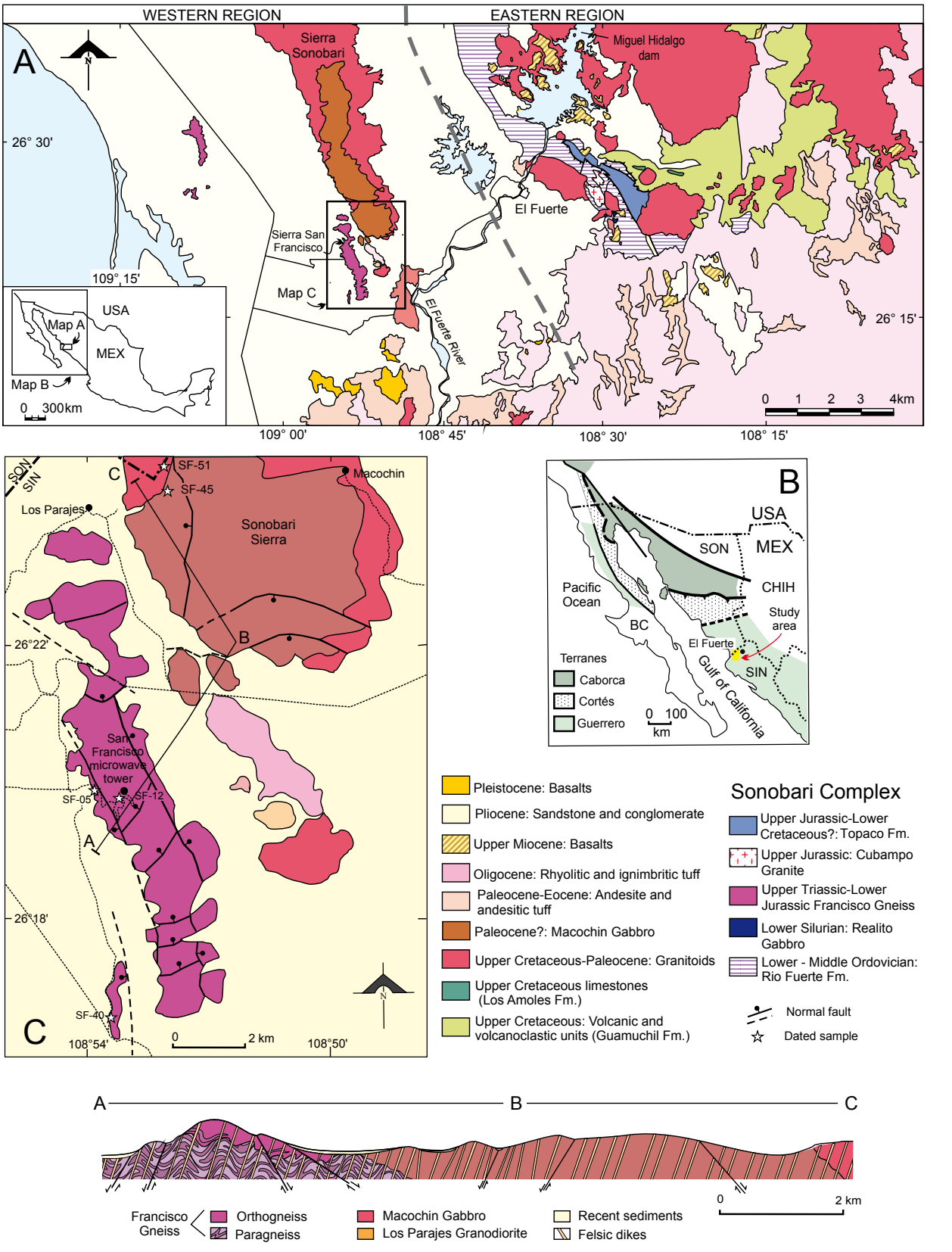

FIGURE 1 A) Geological map of northwestern México. Modified from the 1:250,000 map by Escamilla-Torres *et al.* (2000); B) Simplified terrane map of northwestern México; C) Geologic map of southern Sierra Sonobari schematic cross section. SON: Sonora; CHIH: Chihuahua; BC: Baja California; SIN: Sinaloa; USA: United States of America; MEX: México.

Macochin Intrusion and the Francisco Gneiss are intruded by numerous undeformed aplite and pegmatite dikes of unknown age.

ANALYTICAL METHODS

U-Pb Methodology

For U-Pb geochronology, samples about 5kg were crushed and its minerals separated following common techniques such as jaw crushing, milling, Wilfley separation, Frantz magnetic separation, and heavy liquids (see Solari *et al.*, 2007). The zircon concentrates were carefully studied under a binocular microscope. Between 50 and 150 crystals were carefully selected from each sample in order to obtain all the variations in size, morphology, shape, and color. They were mounted in epoxy resin, ground to expose roughly half of the crystal, and then imaged by cathodoluminescence (CL) using an ELM 3R luminoscope (Marshall, 1988).

Laser Ablation Inductively Coupled Plasma Mass Spectrometry (LA-ICPMS) U-Pb analyses were performed at Laboratorio de Estudios Isotópicos (LEI), Centro de Geociencias, Universidad Nacional Autónoma de México (UNAM), using a Resonetics "Resolution M50" 193nm excimer laser workstation coupled with a Thermo XII Series quadrupole mass spectrometer. The analytical setup and methodology employed in this study are described in Solari *et al.* (2010) and modified as follows: 25s of gas background acquisition was followed by 30s of ablation, carried out in a He atmosphere, employing 140mJ of laser energy, corresponding to an on-target fluence of about 6J/cm^2, a spot 32μm in diameter, and a repetition rate of 5Hz, generating a drill rate of ~0.7μm/s. The acquisition sequence involved an alternation of two analyses of Plešovice reference zircon (~337Ma, Sláma *et al.*, 2008), a NIST 610 standard glass, and five unknown zircons, using a standard-unknown bracketing method (*e.g.* Solari *et al.*, 2010) to allow down-hole fractionation corrections to be performed using a software application developed in-house (Solari and Tanner, 2011). The NIST 610 glass standard was used to recalculate the concentrations of interest, for instance U and Th, by normalizing such elements with ^{29}Si. Other isotopes are observed during analysis, such as P, Ti, and REE, to monitor the presence of inclusions, and when necessary avoid them in the calculation, and to produce zircon REE patterns, which can be helpful for interpreting the calculated ages. Recalculated values Table I (Electronic Appendix, available at www.geologica-acta.com). The precision of the measured ^{207}Pb/^{206}Pb, ^{206}Pb/^{238}U, and ^{208}Pb/^{232}Th ratio errors on the standard zircon was, during these experiments, averaging ~0.86%, 0.48%, and 1.4%, respectively. These errors are quadratically added to the obtained uncertainties for the respective ratios and included in the quoted uncertainties for individual analyses of the analyzed zircons. ^{204}Pb was not monitored during these analyses because its signal was muffled by the ^{204}Hg contained in the carrier gases. Common Pb correction was thus performed by employing the algebraic method of Andersen (2002). A first filter was then applied to ensure the quality of selected analyses, consisting in evaluation of the concordance. For grains with ages of <1000Ma, the analysis was considered concordant if the ^{206}Pb/^{238}U and ^{207}Pb/^{235}U ages differed by less than 10%. For the grains with ages >1000 Ma, the same test was carried out considering ^{206}Pb/^{238}U and ^{207}Pb/^{206}Pb ages. A second filter was then applied using the elemental analysis, especially screening for those elements, such as P and La, the presence of which could indicate some inclusion, for instance apatite, hit during ablation. Those suspicious analyses were thus eliminated. The concordia, age-error, and probability density plots were performed using Isoplot v. 3.70 (Ludwig, 2008). REE zircon patterns were normalized to chondrite values of McDonough and Sun (1995).

^{40}Ar/^{39}Ar Methodology

The ^{40}Ar-^{39}Ar experiments were conducted at the Geochronology Laboratory of CICESE using a Coherent Ar-ion Innova 370 laser extraction system on line with a VG5400 mass spectrometer. The sample preparation procedure consisted of crushing and sieving the sample and then rinsing it with distilled water followed by 98% acetone. Subsequently, the samples were dried overnight at ~60°C. The minerals were then concentrated using the Frantz magnetic separator. To insure >99% purity, the samples were selected by handpicking under a binocular microscope. As the irradiation monitor, aliquots of sanidine FCT 2 (27.84 ± 0.0Ma) were irradiated alongside the samples. The samples were shielded with a Cd-Liner whilst being irradiated for 10hrs at the U-enriched research reactor of the University of McMaster in Hamilton, Ontario. Upon irradiation, the monitors were fused in one step, while the samples were step-heated. The argon experiments were preceded by a blank measurement, with all the argon masses being determined. Upon blank subtraction, the argon isotopes were corrected for radioactive decay, mass discrimination, and calcium, potassium, and chlorine neutron-induced interference reactions. In processing the data, the decay constants and isotopic compositions recommended by Steiger and Jäger (1977) were used. Equations given by York *et al.* (2004) were used in the straight-line calculations. Relevant ^{40}Ar-^{39}Ar data of the experiments, $^{37}Ar_{Ca}/^{39}Ar_K$ diagrams, and the ^{36}Ar/^{40}Ar versus ^{39}Ar/^{40}Ar correlation diagrams for each sample are given in the data repository (Tables 1, 2). All errors are reported at 2σ level. The errors in the integrated, plateau, and isochron ages include the uncertainty in the irradiation parameter J. Additionally for the plateau and isochron ages, the goodness of fit was included

TABLE 1 | Major (wt %) and trace (ppm) element analyses of Sonobari rocks

	Francisco Gneiss amphibolites					Macochin Gabbro		
Sample	SF-9	SF-11	SF-13	SF-14	SF-42	SF-45	SF-46	SF-49
SiO_2 (wt %)	51.5	49.8	48.1	47.6	46.2	47.3	44	45.5
TiO_2	1.47	1.81	1.53	1.57	1.91	1.05	2.09	1.63
Al_2O_3	14.15	15.5	16.25	15.3	14.75	21.9	15	14.25
Fe_2O_3	15.8	12.1	11.7	12.2	14.1	6.86	12.9	12.1
MnO	0.22	0.19	0.23	0.22	0.28	0.08	0.15	0.15
MgO	4.56	5.78	5.74	6.26	7.15	4.93	10.5	11.4
CaO	7.16	8.86	10.2	10.1	10.05	10.35	10.4	10.3
Na_2O	1.38	3.16	3.23	2.95	2.31	3.34	2.24	1.88
K_2O	1.24	0.57	0.86	0.85	0.66	0.8	0.51	0.86
P_2O_5	0.3	0.24	0.21	0.18	0.21	0.08	0.04	0.12
LOI	1.5	1	0.98	1.17	1.28	2.5	0.19	1.6
Total	99.3	99.1	99.1	98.5	99	99.3	98.1	99.9
CIPW								
Q	10.8	1.5	0.0	0.0	0.0	0.0	0.0	0.0
or	7.9	3.5	5.3	5.2	4.1	4.9	3.1	5.2
ab	13.3	29.5	30.0	27.7	21.8	29.2	19.0	17.3
an	30.9	27.5	28.2	27.2	29.3	43.6	30.2	28.5
ne	0.0	0.0	0.0	0.0	0.0	1.0	1.0	0.0
di	4.1	13.3	18.1	19.2	17.3	6.9	18.1	18.3
hy	26.7	18.0	2.4	5.8	13.3	0.0	0.0	4.7
ol	0.0	0.0	10.0	8.8	7.2	10.1	21.6	20.1
mt	3.3	3.6	3.3	3.4	3.7	2.7	3.9	3.3
il	2.2	2.6	2.2	2.3	2.8	1.5	3.0	2.3
ap	0.7	0.5	0.5	0.4	0.5	0.2	0.1	0.3
Rb (ppm)	33.4	9	10.4	14.2	13	12.2	5.5	14.9
Sr	124	247	303	256	232	689	262	234
Ba	258	208	258	98.4	205	521	185.5	420
Co	29.2	30.2	30.1	37.3	46.4	29.5	51.5	52.3
Cu	8	155	76	15	123	79	78	85
Cr	40	120	180	200	160	10	150	180
Ni	46	61	45	63	74	22	71	104
V	415	281	304	327	360	253	529	507
Zn	79	55	105	92	129	70	121	117
Zr	109	115	98	93	112	28	52	57
Y	28	29.8	28	29.2	32.6	13.7	27.2	26.4
Nb	3.8	3.1	2.7	2.5	1.8	2.8	4.5	2.9
Th	3.43	1.21	1.05	0.57	0.24	0.46	0.26	0.3
Ta	0.2	0.2	0.2	0.1	0.1	0.2	0.2	0.1
U	1.13	0.4	0.68	1.04	0.1	0.2	0.12	0.11
Pb	4	4	4	4	4	7	4	4
Hf	3.4	3.3	2.7	2.6	3	1.1	2	2.1
La	14.9	9.5	8.1	6.5	5.5	5.1	6.3	6.2
Ce	32.7	23.6	19	16.5	15.3	13	19	18.4
Pr	4.6	3.6	2.86	2.63	2.67	2.05	3.25	3.19
Nd	19.5	17	13.6	12.7	13.6	10	16.8	16
Sm	4.73	4.83	3.96	3.83	4.46	2.71	5.18	4.93
Eu	1.38	1.64	1.34	1.35	1.62	0.93	1.45	1.43
Gd	4.95	5.42	4.58	4.54	5.31	2.82	5.4	5.5
Tb	0.91	0.99	0.88	0.86	1	0.5	0.88	0.93
Dy	5.37	6.11	5.32	5.28	6.18	2.83	5.55	5.23
Ho	1.16	1.29	1.15	1.15	1.32	0.57	1.09	1.07
Er	3.32	3.64	3.33	3.42	3.76	1.62	3.03	2.88
Tm	0.54	0.58	0.53	0.54	0.59	0.24	0.38	0.42
Yb	3.2	3.23	3.08	3.41	3.49	1.33	2.41	2.43
Lu	0.51	0.5	0.51	0.56	0.53	0.2	0.36	0.36

in the age uncertainty whenever the mean square weighted deviation (MSWD) exceeded a value of one. The integrated ages were calculated by adding the fractions of the step-heating experiments. Plateau ages were calculated with the weighted mean of three or more consecutive fractions, which were in agreement within 2σ errors excluding the uncertainty in irradiation parameter (J).

Geochemistry methodology

For geochemical study, the samples were first ground in a steel jaw crusher and then finely powdered in an agate grinder. Major and trace elements were quantified by inductively coupled plasma atomic emission spectrometry (ICP-AES) and rare earth elements (REEs) and additional

TABLE 2 | VG5400 Ar-Ar laser step heating experiments SF-40 hornblende

Pwr	$^{39}Ar \times 10^{-6}$	F ^{39}Ar	$^{40}Ar^*/^{39}Ar_K$	Age in Ma			% $^{40}Ar^*$	$^{40}Ar/^{36}Ar$	$^{37}Ar_{Ca}/^{39}Ar_K$
0.20	2.605	0.0019	17.76 ± 5.26	105.2 ± 30.2	a	‡	18.92	364.45	0.88
0.50	6.378	0.0047	77.89 ± 3.43	421.8 ± 16.6	b		59.69	733.06	1.66
0.80	6.757	0.0050	26.17 ± 2.16	153.0 ± 12.1	c		73.81	1128.23	2.30
1.35	41.970	0.0309	12.37 ± 0.45	73.9 ± 2.6	d		85.25	2002.93	4.07
2.00	510.719	0.3762	13.49 ± 0.10	80.5 ± 0.6	e		93.05	4251.05	4.39
2.55	350.564	0.2582	12.28 ± 0.06	73.4 ± 0.3	f		93.35	4441.91	4.27
3.70	299.721	0.2208	12.92 ± 0.09	77.2 ± 0.5	g		88.58	2587.01	4.41
6.00	138.751	0.1022	12.87 ± 0.24	76.9 ± 1.4	h		89.51	2817.24	4.61

Irradiation parameter J= 0.003382 ± 0.000013 (obtained with sanidine FCT 2 (27.84±0.04Ma) irradiated alongside the samples).

Integrated results

$^{39}Ar \times 10^{-6}$	$^{40}Ar^*/^{39}Ar_K$	Age in Ma	% $^{40}Ar^*$	$^{40}Ar/^{36}Ar$	$^{37}Ar_{Ca}/^{39}Ar_K$
1357.0	13.33 ± 0.06	79.54 ± 0.47	89.09	2707.45	4.35

‡ fraction ignored in the isochron age calculation.
The step-heating ages obtained for the eight fractions collected do not fulfill the criteria to calculate a plateau age. Only fractions g and h, which represent 32.30% of the ^{39}Ar released, have ages in agreement within one standard deviation, the weighted mean of these yielded t = 77.14 ± 1.10 Ma, the MSWD obtained was 0.04.
The $^{37}Ar_{Ca}/^{39}Ar_K$ diagram indicates that the sample has a uniform composition with respect to its Ca/K content.
The line defined with fractions b to h in the correlation diagram (Figure 5) indicates the presence of excess argon with a $(^{40}Ar/^{36}Ar)_i$ = 680 ± 91, therefore, the best estimate for the age of this sample is the isochron age calculated from the correlation diagram: t_c = 66.94 ± 4.84 Ma; MSWD = 6.1 for n = 7.

trace elements were obtained for a subset of samples by inductively coupled plasma-mass spectrometry (ICP-MS) at ALS Minerals commercial laboratory in Vancouver, Canada. Sample decomposition was performed using lithium metaborate/lithium tetraborate ($LiBO_2/Li_2B_4O_7$) for ICP-AES and lithium metaborate fusion for ICP-MS. The lower detection limit is 0.01% for major elements and 0.1 to 5ppm for trace elements.

GEOLOGICAL UNITS

Francisco Gneiss

This unit is mainly composed of paragneiss, orthogneiss and amphibolite. Paragneisses crop out mainly in the western slope of the San Francisco Sierra, where they are intercalated with scarce thin layers of biotite-rich or muscovite-rich schists and conglomerate gneisses, indicating a sedimentary protolith. Migmatization occurs as a stromatic structure, depicted by bands of leucosome developed along a pervasive foliation S1 (Fig. 2A, B). In thin section, the paragneisses consist of quartz, plagioclase, K-feldspar, variable amounts of biotite, amphibole, epidote-zoisite ± muscovite, with accessory rutile, titanite, zircon, and occasional garnet (Fig. 3A). The main fabric is a foliation indicated by the preferred orientation of amphibole and biotite crystals.

The orthogneiss crops out as decametric bodies that include meter-scale xenoliths of the paragneisses. In thin section, the orthogneiss consists of plagioclase, quartz, K-feldspar, biotite, epidote, with minor apatite and zircon. The estimated modal content indicates that the protolith was a granodiorite, which is consistent with previous chemical analyses of felsic rocks in the area (Keppie *et al.*, 2006). The orthogneiss display a mylonitic foliation indicated by elongation of dynamic recrystallized quartz and preferred orientation of biotite (Fig. 3B).

The orthogneiss and paragneisses are intercalated with numerous bands of amphibolite. Field relationships indicate that the amphibolite protolith corresponds to mafic dikes that crosscut previous rocks (Fig. 2C). In thin section, the amphibolites consist of plagioclase, amphibole, minor biotite, titanite, rutile, epidote-zoisite, apatite, and secondary chlorite after amphibole and biotite (Fig. 3C). The samples SF-9 and SF-11 have quartz in addition to the minerals mentioned above. The main fabric in amphibolites is originated by preferred orientation of amphibole, biotite, and plagioclase. Migmatization in the orthogneisses and amphibolites is indicated by centimeter-thick leucosome bands (Fig. 2D), which follow the S2 foliation.

Structure

The paragneisses display a penetrative foliation along which, thin and laterally persistent bands of leucosome

occur, producing a stromatic structure locally. The main field fabric of the orthogneisses and amphibolites is a pervasive foliation (S2). A previous planar fabric (S1) of the paragneisses is rotated and becomes sub-parallel to S2. Subsequently, the S2 foliation is refolded by tight overturned folds (F3) with NNE vergence (Fig. 2B). The last phase of folding (F4) yields open folds with upright axial planes.

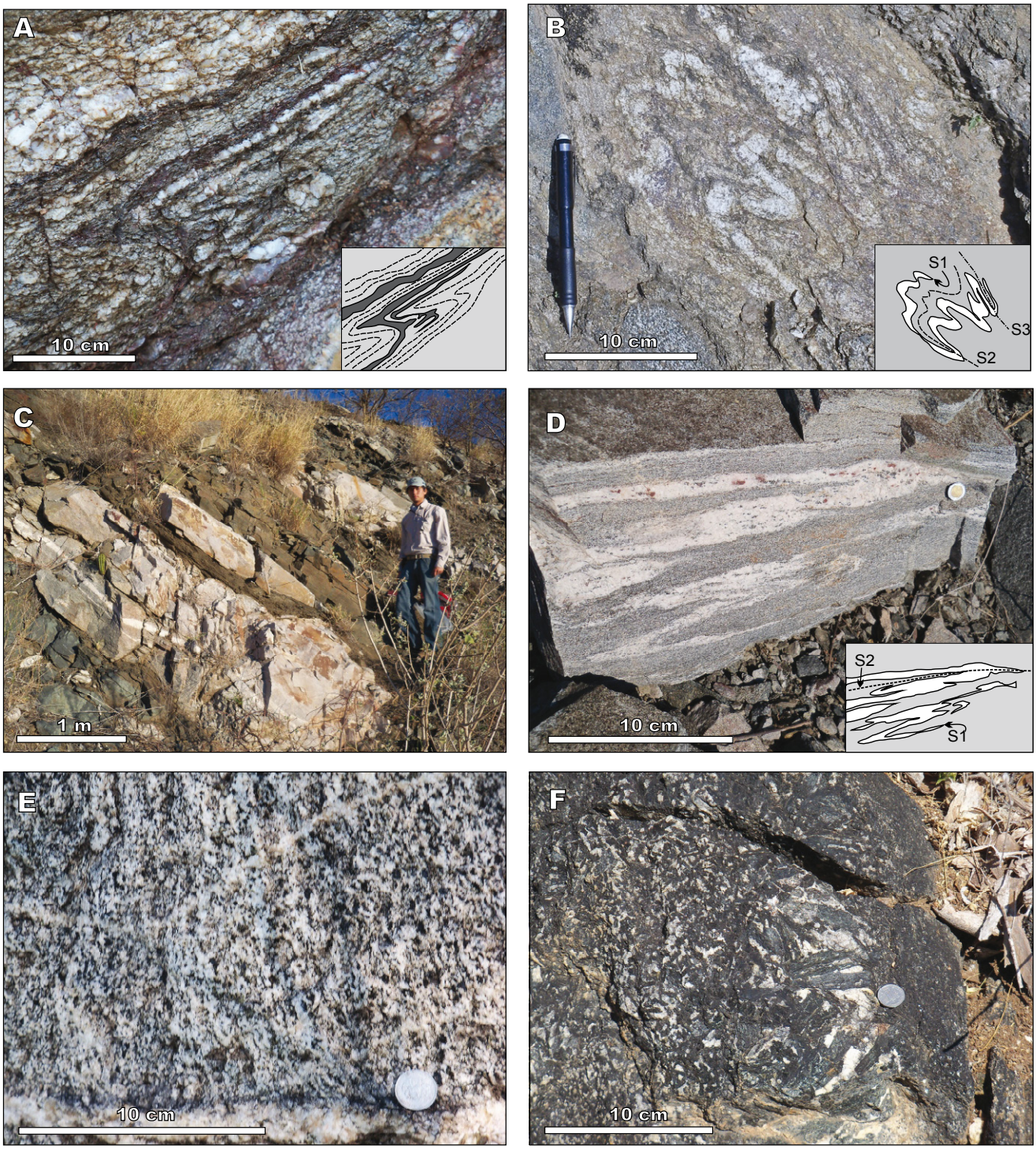

FIGURE 2 Photographs of the Francisco Gneiss and intruding igneous rocks: A) Folded intercalations of quartz-feldspathic paragneiss and micaschists; B) Refolded paragneiss, with indications of S1, S2, S3 foliations; C) Amphibolite transecting orthogneiss; D) Sub-isoclinally folded leucosome in orthogneiss; E) The Los Parajes Granodiorite; F) Hornblende-plagioclase gabbro of the Macochin Gabbro, with pegmatitic pods.

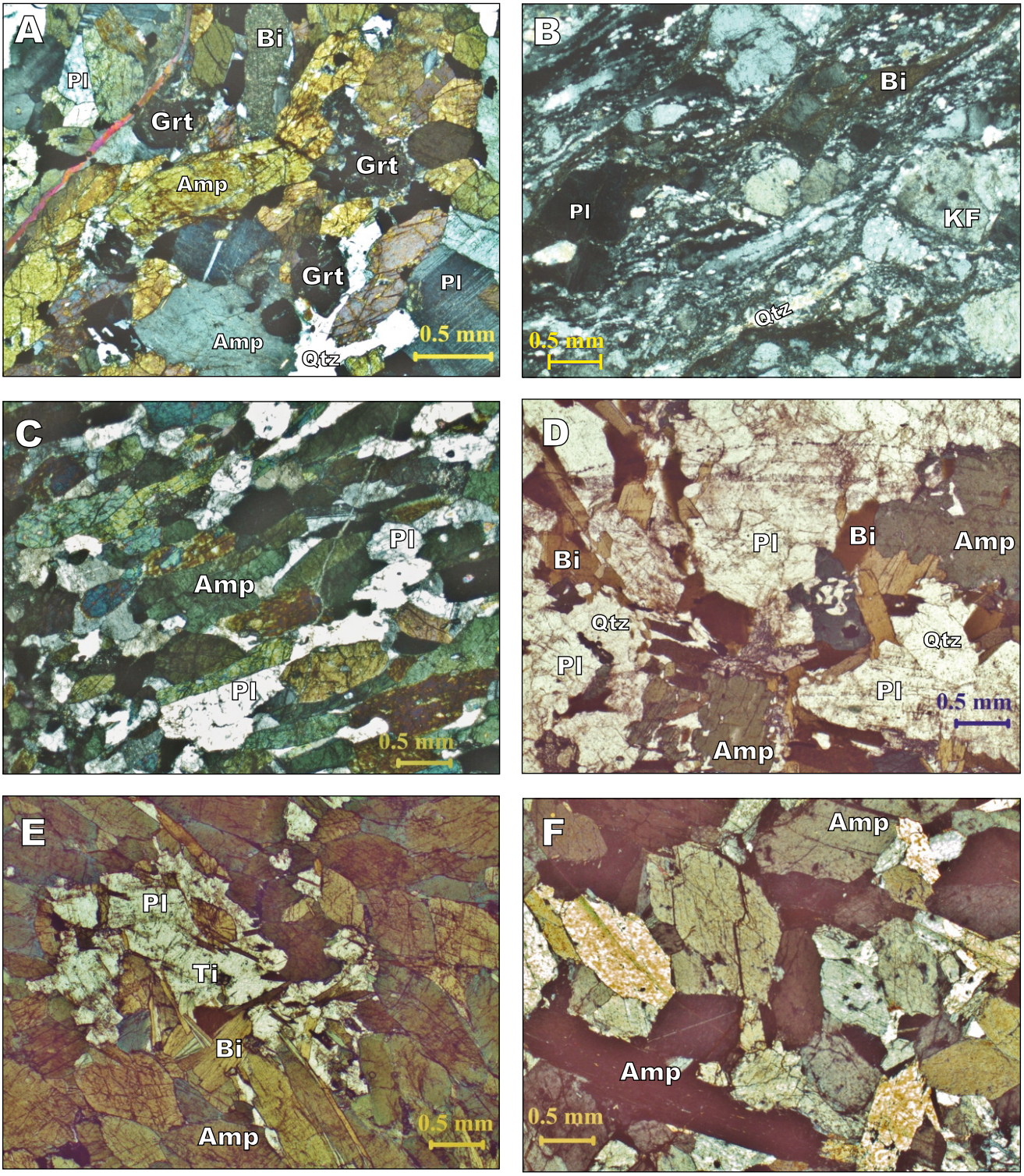

FIGURE 3 Thin section photographs of: A) Francisco paragneiss consisting of amphibole (Amp), plagioclase (Pl), quartz (Qtz), biotite (Bi), garnet (Grt) and titanite (Ti); NP = non-polarized light; PL = polarized light. B) Mylonitic orthogneiss displaying dynamic recrystallized bands of quartz and feldspar, and porphyroclasts of K-feldspar (KF), plagioclase (Pl) and biotite; C) Amphibolite from the Francisco Gneiss formed of amphibole and plagioclase with minor biotite; minerals are aligned along a continuous foliation (NP); D) The Los Parajes Granodiorite consisting of plagioclase, quartz, amphibole, biotite, minor epidote and opaques, with a hypidomorphic texture (NP); E) Macochin Gabbro made by clusters of plagioclase with minor biotite surrounded by amphibole crystals (PL); F) Cumulate of amphibole crystals in the base of the Macochin Gabbro (PL).

Los Parajes Granodiorite

This unit is made up of bodies of granodiorite exposed in the southern Sierra Sonobari (Fig. 2E). In thin section, this granodiorite consists of coarse-grained plagioclase, quartz, K-feldspar, hornblende, biotite, with minor epidote-clinozoisite, apatite, and zircon (Fig. 3D). Chlorite locally replaces amphibole. Crystals vary from euhedral to anhedral, producing a hypidiomorphic granular texture.

Macochin Gabbro

This unit consists mainly of medium to coarse-grained mafic rocks composed of amphibole and plagioclase, which contain pegmatitic pods with amphibole crystals up to 12cm in length (Fig. 2F). Weathered amphibole cumulates with strong retrogression to chlorite occur in the lower part of the unit (Fig. 3F). Locally, the hornblende-plagioclase gabbro remains as lensoid bodies transected by numerous non-foliated felsic aplitic and pegmatite dikes. In thin section, the gabbro mostly consists of green amphibole and plagioclase, with minor biotite and epidote-zoisite. Rutile occurs as an accessory mineral surrounded by titanite reaction rims. Minor secondary chlorite occurs after biotite. The texture is mostly hypidiomorphic granular, but plagioclase is locally grouped, forming a mottled texture (Fig. 3E).

The contact between the Macochin Gabbro and the Francisco Gneiss occurs in the southern Sierra Sonobari foothills, where it is covered by recent sediments. Although Mullan (1978) indicates that the Río Fuerte Formation is exposed near that contact, rocks of this unit were not found in the area. The contact between the Los Parajes Granodiorite and the Macochin Gabbro, although poorly exposed, is interpreted as an intrusion of the gabbro in the granodiorite.

RESULTS

U-Pb geochronology

Three samples were dated with U-Pb geochronology, namely paragneiss (SF-05) and orthogneiss (SF-12) from the Francisco Gneiss, and an undeformed granodiorite sample (SF-51) from the Los Parajes Granodiorite.

Paragneiss

The sample studied (SF-05) is a quartz-K-feldspar-plagioclase-biotite paragneiss from the western slope of the San Francisco Sierra (Fig. 1C). Zircons separated from this sample display various sizes (ca. 50 to >250μm) and colors, ranging from colorless to dark red and honey. Ovoid shape prevails, although some elongate grains are present. Almost all of them present polished and rounded terminations produced by the sedimentary transport prior to their deposition (Fig. 4). The cathodoluminescence imaging reveals cores and variably developed rims, generally with contrasting luminescence and sector-zoning crystallization. From the 120 analyses performed, 102 meet the criteria defined above, yielding concordant to variably discordant ages (Fig. 4A) from Middle Ordovician to Paleoproterozoic. Up to 95% of the ages are Proterozoic, and 83% are older than 1Ga. The main peaks of the relative probability plot yield average ages of 1690 and 1404Ma, while minor peaks yield ages of 1156, 921, and 517Ma (Fig. 4B). Five grains yield discordant ages older than 2Ga. The four youngest overlapping zircons yield a Middle Cambrian mean average age of 509 ± 29Ma (Fig. 4A, inset), which is regarded as the maximum age of deposition for sample SF-05.

Orthogneiss

An orthogneiss sample belonging to the Francisco Gneiss (SF-12) exposed in the middle-upper part of the western slope of the San Francisco Sierra was dated with the U-Pb method. Zircons separated from this sample are up to 220μm in size and slightly yellow colored. Stubby to ovoid shapes prevail, although some prismatic shapes with pyramidal terminations are also present (Fig. 4). However, most of the grains are rounded, which can be an effect related to the degree of metamorphism these zircons underwent after their magmatic crystallization. In general, under cathodoluminescence they show oscillatory to sector zoning growths. Some inherited cores are evident, as well as signs of resorption. Due to the internal complexity of zircons belonging to this sample, we performed 60 analyses, of which 10 are excluded following the criteria enlisted in the analytical methods section (Table 3). Several of the remaining analyses are variably discordant, probably as a result of Pb loss during high grade metamorphism, which is also suggested by some disturbed REE patterns (*e.g.* zircon analysis # 10 in Table I; Fig. 4C, inset). Most of the analyses straddle the concordia plot between 220 and ca. 185Ma (Fig. 5C). The true crystallization age can be interpreted as indicated by: i) the upper intercept of the discordia at 248 ± 28Ma; ii) the average of the $^{206}Pb/^{238}U$ ages straddling the concordia at roughly 195Ma (not shown). In the first case, all of the analyzed zircons are variably affected by Pb loss, and their ages only indicate a minimum age of magmatism. In the second case all those analyses roughly between 220 and ca. 200Ma would represent variable amounts of inheritance and/or the first zircons crystallizing in the magma chamber. Our interpretation for the sample SF-12 favors a crystallization age of 248 ± 28Ma. Subsequent metamorphism evidenced by overgrowths in the cathodoluminescence images (Fig.

TABLE 3 | VG5400 Ar-Ar laser step heating experiments SF-45 hornblende small

Pwr	$^{39}Ar \times 10^{-6}$	F ^{39}Ar	$^{40}Ar^*/^{39}Ar_K$	Age in Ma			% $^{40}Ar^*$	$^{40}Ar/^{36}Ar$	$^{37}Ar_{Ca}/^{39}Ar_K$
0.20	2.984	0.0059	33.05 ± 5.33	191.20 ± 29.24	a	‡	30.48	425.07	0.777
0.50	5.935	0.0118	49.72 ± 6.51	280.40 ± 34.01	b	‡	33.39	443.64	2.223
0.80	8.081	0.0161	2.50 ± 1.43	15.20 ± 8.64	c	‡	6.24	315.17	1.374
1.35	22.133	0.0440	7.02 ± 0.94	42.32 ± 5.57	d	‡	31.51	431.45	6.357
1.95	138.498	0.2754	7.61 ± 0.14	45.82 ± 0.86	e	‡	61.83	774.23	11.531
2.55	191.759	0.3813	8.23 ± 0.08	49.53 ± 0.47	f		72.75	1084.51	12.436
3.10	66.168	0.1316	8.23 ± 0.34	49.51 ± 2.00	g		83.49	1789.59	11.815
3.70	23.748	0.0472	8.30 ± 0.45	49.95 ± 2.64	h		97.19	10513.06	11.319
7.50	43.566	0.0866	7.45 ± 0.45	44.88 ± 2.65	i		89.27	2754.41	11.542

Irradiation parameter J= 0.003382 ± 0.000013 (obtained with sanidine FCT 2 (27.84±0.04Ma), irradiated alongside the samples).

Integrated results

$^{39}Ar \times 10^{-6}$	$^{40}Ar^*/^{39}Ar_K$	Age in Ma	% $^{40}Ar^*$	$^{40}Ar/^{36}Ar$	$^{37}Ar_{Ca}/^{39}Ar_K$
502.9	8.49 ± 0.13	51.04 ± 0.79	59.97	738.14	11.340

‡ fractions ignored in the isochron age calculation.
The best estimate for the age of this sample is taken form the plateau age, which was calculated with the weighted mean of fractions f to i t_p = 49.40 ± 0.96 Ma, 64.67 % of ^{39}Ar released in 4 consecutive fractions, MSWD = 1.00.
The distribution of the plateau fractions in the correlation diagram (Figure 5) yields an isochron age of 47.4 ± 4.52Ma, this age is within errors, in agreement with the plateau age.

5) cannot be dated, but prevent to obtain a better resolution of the rock age.

Los Parajes Granodiorite

The Los Parajes Granodiorite (SF-51) contains prismatic zircons that are quite large (up to 300μm) with well-developed bipyramidal terminations. Under cathodoluminescence they show oscillatory zoning, with overgrowths parallel to the crystal shape (Fig. 4). Gray-yellowish inclusions, up to 30μm in size, are often present, and are interpreted as a phosphate phase. Together with their REE contents, whose typical enrichments in HREE, positive Ce and Sm anomalies, and negative Pr and Eu anomalies are suggestive of igneous crystallization (Fig. 4D, inset; Hoskin and Schaltegger, 2003, and references therein), the cathodoluminescence imaging also supports igneous growth for the imaged zircons. Thirty-two analyses met the exclusion criteria indicated above. Most of the ages are concordant to slightly discordant within analytical error, with a mean $^{206}Pb/^{238}U$ of 64 ± 1Ma, which is interpreted as the crystallization age of the granodiorite (Fig. 4D).

$^{40}Ar/^{39}Ar$ geochronology

Two samples were dated with $^{40}Ar/^{39}Ar$ geochronology, an amphibolite from the Francisco Gneiss (SF-40) and an amphibole-plagioclase gabbro (SF-45) from the Macochin Gabbro.

Francisco Gneiss amphibolite

Sample SF-40 was collected from the western slope of the San Francisco Sierra. From the results obtained for the amphibole concentrate it is deduced that the age spectrum (Fig. 5A) presents some argon perturbation. The eight fractions collected did not fulfill the criteria for calculating a plateau age. Only the last two fractions, which represent 32.30% of the ^{39}Ar released, have ages in agreement within one standard deviation; their weighted mean (MSWD = 0.4) yielded an age of 77 ± 2Ma. The $^{37}ArCa/^{39}Ar_K$ diagram yielded values indicating a uniform composition of Ca/K ~ 9. Some fractions yielded ages well in excess of the expected age; furthermore, seven of the eight data points define a straight line in the $^{36}Ar/^{40}Ar$ versus $^{39}Ar/^{40}Ar$ correlation diagram. The y-intercept yielded $(^{40}Ar/^{36}Ar)_i$ = 680 ± 91, confirming the presence of excess argon. On the basis of the distribution of the data points in the correlation diagram (Fig. 5B) we have confidence in the straight line defined even though MSWD = 6.1, and therefore our preferred age for sample SF-40 is an isochron age of 67 ± 5Ma.

Macochin Gabbro

Sample SF-45 is a medium-grained amphibole-plagioclase gabbro from the Macochin Gabbro. This rock displays an inequigranular texture, containing pods of amphibole-plagioclase megacrystals. The amphibole concentrate prepared from the megacrystals was labeled

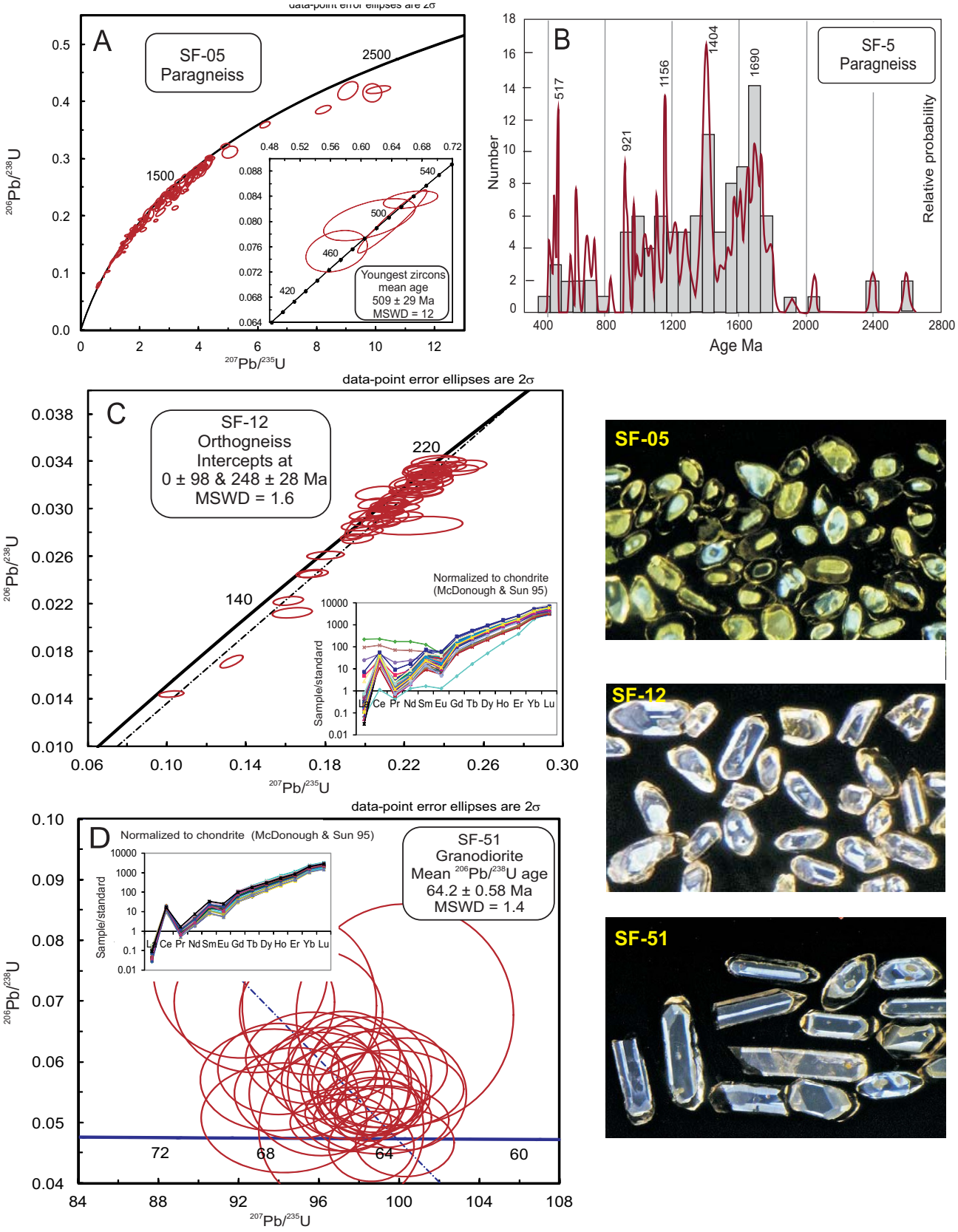

FIGURE 4 Results of the U-Pb geochronology. A) Concordia diagram for the paragneiss zircon ages; inset with the youngest zircon ages; B) Relative probability plot for the paragneiss; C) Concordia diagram of the orthogneiss; inset with the REE pattern of zircons; D) Concordia diagram for the Los Parajes Granodiorite; inset with the REE patterns of zircons. Right: selected zircons from each sample.

SF-45a and the amphibole concentrate prepared from the medium-grained fraction was labeled SF-45b. The age spectrum obtained for sample SF-45a is presented in Figure 5C; eight fractions were collected in the step-heating experiment. The integrated age for this sample is not reported because, due to analytical problems, mass 36 could not be evaluated for the fraction released with 3.20W of laser power; therefore, no age was calculated for this fraction. However, since this fraction only represents 3.67% of the total ^{39}Ar released, it is not critical for the interpretation of the age of the sample. The bulk of the ^{39}Ar (87.88%) was released in three fractions, which are identified with an arrow in Figure 5B. A 55 ± 4Ma age was obtained from the weighted mean of their individual ages. These three fractions are characterized by Ca/K ~ 25. The data define a straight line in the (^{36}Ar/^{40}Ar) versus (^{39}Ar/^{40}Ar) correlation diagram, which yields a less precise isochron age of 54 ± 10Ma (Fig. 5D); the (^{40}Ar/^{36}Ar) obtained from the y-intercept is, within error, of atmospheric composition. Our preferred age for sample SF-45a is the plateau age of 55 ± 4Ma. Sample SF-45b yielded results comparable with those of sample SF-45a (Fig. 5E, F). A plateau age of 49 ± 1Ma is defined by four consecutive fractions which represent 64.67% of the 39Ar released; the plateau segment is characterized by a Ca/K value of ~22. The data were plotted in the (^{36}Ar/^{40}Ar) versus (^{39}Ar/^{40}Ar) correlation diagram, and the plateau fractions define an isochron age of 47 ± 5Ma, which is slightly younger than the plateau age. Considering all the data, the isochron ages of samples SF-45b and SF-45a overlap each other within the margin of error, consequently can be considered as indicating the same age. Alternatively, the younger ages in small grains could be related to partial resetting by later events, because Ar diffusion is easier in small grains than in larger grains (*e.g.* Maurel *et al.*, 2003).

Geochemistry

Major, trace, and Rare Earth Element (REE) contents of eight samples from the Sierra Sonobari are included in Table 3. Major element compositions were normalized to 100% on a volatile-free basis for all plotting purposes. All rocks display coherent distribution of major elements; therefore, metamorphism of the Francisco Gneiss is assumed to be mostly isochemical.

Major elements

Mafic rocks of the Francisco Gneiss and the Macochin Gabbro display a similar distribution of major elements despite the age difference. Both are characterized by relatively high values of titanium (1–2%) and low values of alumina (14–16%), except for the pegmatitic gabbro (21%). According to the Total Alkali Silica (TAS) diagram (Fig.

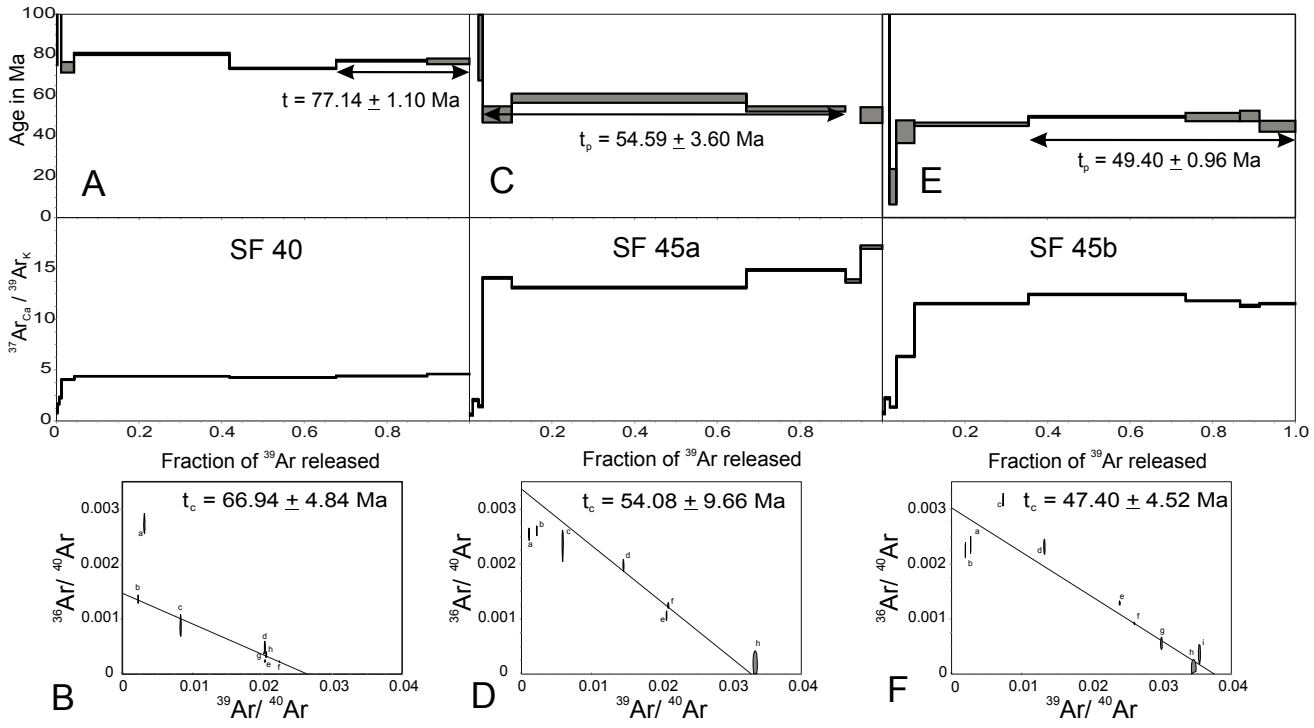

FIGURE 5 | From top to bottom: age spectra, $^{37}Ar_{Ca}/^{39}Ar_K$ diagram, and ^{36}Ar/^{40}Ar versus ^{39}Ar/^{40}Ar correlation diagram for: A-B) Amphibolite of the Francisco Gneiss; C-D) Coarse-grained amphibole of the Macochin Gabbro; E-F) Fine-grained amphibole of the Macochin Gabbro. Arrows indicate the segment selected for plateau calculation. Preferred ages are highlighted in bold typeface. Errors are reported in 2σ.

6A), data from both units fall around the discrimination line separating the alkaline and subalkaline fields, corresponding to gabbroic peridotite, gabbro, and gabbro-diorite. The diagram by Winchester and Floyd (1977, Fig. 6B), which uses incompatible elements (Rollinson, 1993), yields the same results as the TAS diagram, suggesting that significant mobility of major elements did not occur, even if the Francisco Gneiss underwent amphibolite facies metamorphism. In this regard, the CIPW norm shows that mafic rocks of both units are mainly olivine tholeiites (Fig. 6C), although some samples of the Macochin Gabbro are undersaturated, with normative nepheline, such as alkaline-olivine gabbros, while some amphibolites of the Francisco Gneiss are oversaturated varieties or quartz tholeiites. The high FeOt/MgO in the gabbros of both units indicates a tholeiitic affinity (Fig. 6D). This geochemical trend is consistent with the proportions of alkalis observed in the AFM diagram (Fig. 6E).

Trace elements

The rare earth patterns of the mafic rocks of the Francisco Gneiss normalized to the chondrite concentrations of Sun and McDonough (1989) show a relatively flat spectrum, slightly enriched in light rare earth elements (LREE), and a weak negative Eu anomaly for the more differentiated varieties (Fig. 7A). On the other hand, the Macochin Gabbro shows a spectrum dominated by heavy rare earth element (HREE) depletion and a convex shape characteristic of REE concentrations of hornblende, consistent with the dominant presence of this mineral in the Macochin Gabbro.

In the primitive mantle-normalized trace element spider-diagram, the mafic samples have the same high-field-strength element (HFSE) concentrations (MREE, HREE,

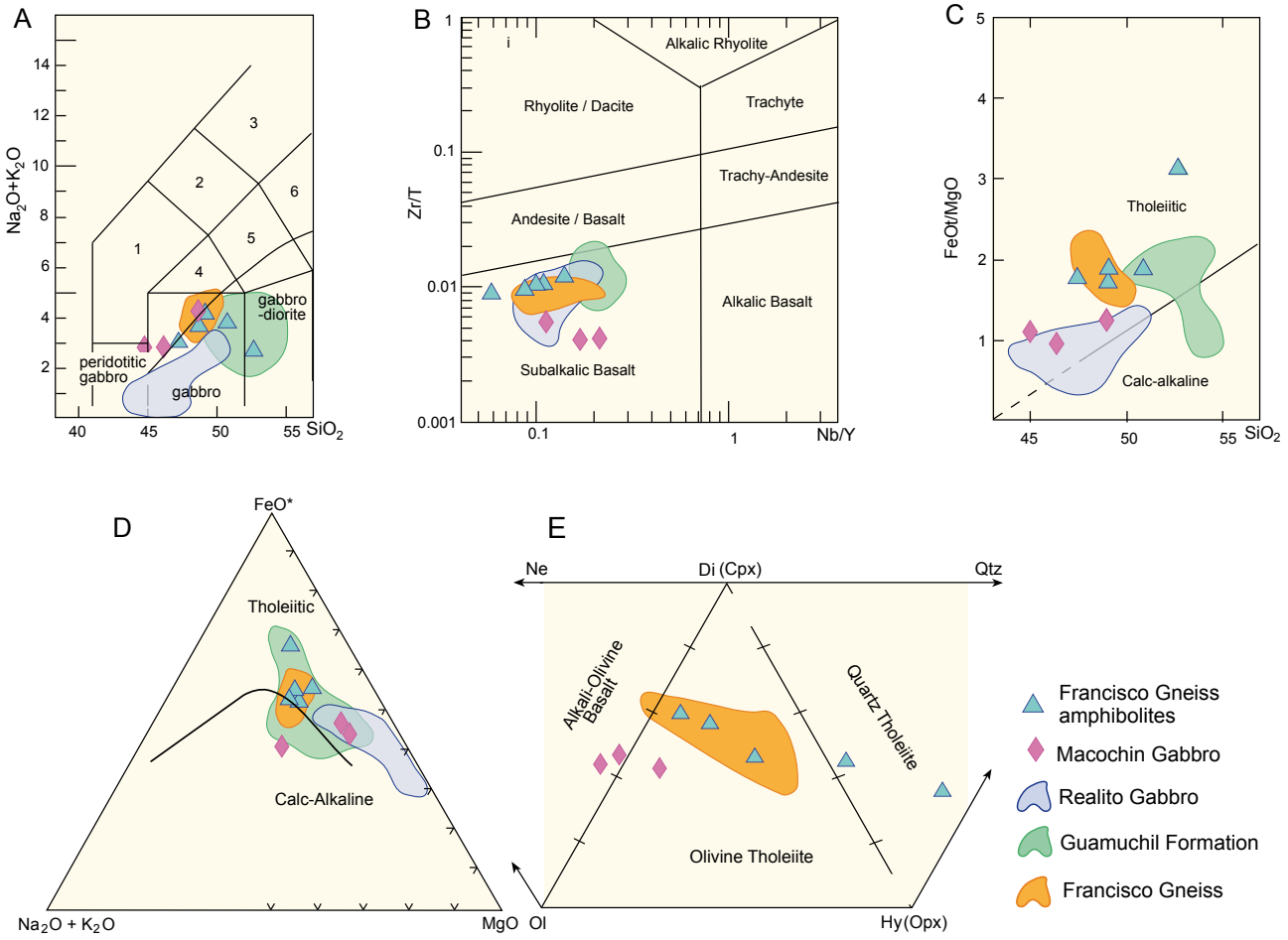

FIGURE 6 Total alkalis vs. SiO_2 diagram for the Sonobari region rocks. The rock classification is after Middlemost (1994). Numbered fields: 1, foid–gabbro; 2, foid–monzodiorite; 3, foid–monzosyenite; 4, monzogabbro; 5, monzodiorite; 6, monzonite. The line separating the alkaline and subalkaline fields is after Miyashiro (1978). B) Zr/Ti vs Nb/Y discrimination diagram (after Winchester and Floyd, 1977; Pearce, 1996). C) FeO_T/MgO vs. SiO_2 discrimination diagram (after Miyashiro, 1974). D) AFM discrimination diagram, dividing line for tholeiitic and calc-alkaline trends (after Irvine and Baragar, 1971). E) Classification of mafic and related basic and ultrabasic magmatic rocks according to their CIPW normative composition expressed as Ne-Ol-Di, Ol-Di-Hy, Di-Hy-Q (after Thompson, 1984). Fields for the Realito Gabbro, Guamuchil Formation (Vega-Granillo *et al.*, 2012) and previous Francisco Gneiss data (Keppie *et al.*, 2006) are shown for comparison.

Y, Ti, and Zr; Fig. 7B) as the oceanic basalts (Saunders and Tarney, 1984). However, a significant enrichment is observed for the rest of the elements, in particular for the large-ion lithophile elements (LILE) that show positive anomalies in Ba, U, K, and Pb. Such enrichment suggests a crustal influence, consistent with a strong Nb and Ta negative anomaly.

DISCUSSION

A first metamorphic-deformation event (M1) yielded a S1 foliation in the paragneisses of the Francisco Gneiss, which was transected by the orthogneiss protolith. Thus the protolith of the Francisco Gneiss is regarded as a metasedimentary sequence intruded by granodiorite, being both types of rocks crosscut by later mafic dikes (Fig. 2C). Subsequently, a metamorphic-deformation event (M2) overprints previous rocks, generating a second foliation (S2). Then, two folding phases overprint previous structures. This interpretation differs from that of Keppie *et al.* (2006), who regard the protolith of this unit as either a bimodal sequence of mafic and felsic flows interbedded with sedimentary rocks or a set of dikes or sills intruding sedimentary rocks.

Provenance

The youngest cluster of zircon ages in the Francisco paragneiss (sample SF-5) has an average age of 509 ± 29Ma, which is considered as the maximum depositional age for this rock. The 248 ± 28Ma intrusion age of the orthogneiss protolith (sample SF-12) represents the upper limit of the sediment deposition. In this context, it should be noted that Triassic and Lower Jurassic sequences from central and northern Sonora mostly contain Late Permian detrital zircons (González-León *et al.*, 2009). Absence of Late Permian zircons in the Francisco paragneiss is consistent with a Paleozoic age of the sedimentary protolith.

More than 83% of the dated zircon grains yield Paleo- and Mesoproterozoic ages. Similar age ranges have been founded in Neoproterozoic and Cambrian sandstones from cratonic and platform sequences of the southwestern North American Cordillera including north-central Sonora (Gehrels and Stewart, 1998; Gross *et al.*, 2000; Stewart *et al.*, 2001; Barbeau *et al.*, 2005). The oldest peak may arise from igneous rocks of the Mojave, Yavapai, and Mazatzal provinces (Fig. 8), occurring in northern Sonora and southern Arizona (Anderson and Silver, 2005). These provinces include igneous and metamorphic rocks dated mainly between 1.8 and 1.6Ga (*e.g.* Amato *et al.*, 2008). The ~1.4Ga peak may come from igneous rocks intruded between 1.48 and 1.35Ga, which are dispersed throughout the Paleo- and Mesoproterozoic crust of southern and eastern Laurentia (Windley, 1993; Van Schmus *et al.*, 1996; Karlstrom and Humphreys, 1998) including northern Sonora (Anderson and Silver, 1981; 2005). Zircon ages between 1.3 and 0.9Ga can be derived from the Grenvillian orogenic belt exposed in the Llano province of Texas, with ages between 1.37 and 1.12Ga (Reese *et al.*, 2000). Magmatic rocks of ca. 1.1Ga intrude the Paleoproterozoic crust of southern Laurentia (*e.g.* Whitmeyer and Karlstrom, 2007), including northwestern Sonora (Anderson and Silver, 1981, 2005). The youngest ages yield a Middle Cambrian mean age (inset in Fig. 4A), which has not been reported from lower Paleozoic sandstones of Sonora or Arizona (*e.g.* Stewart *et al.*, 2001), although a ~500Ma cluster of some

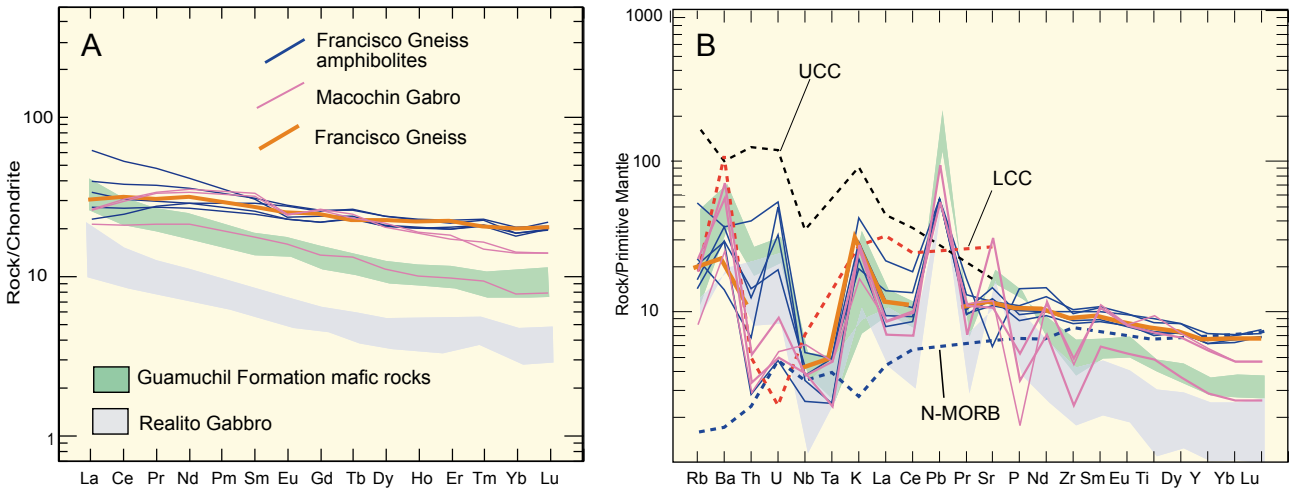

FIGURE 7 A) REE element values normalized to chondrite from Sun and McDonough (1989). Fields for the Realito Gabbro, Guamuchil Formation (Vega-Granillo *et al.*, 2012) and previous Francisco Gneiss data (Keppie *et al.*, 2006) are shown for comparison. B) Trace element values normalized to Primitive Mantle from Sun and McDonough (1989) compared to average N-type MORB, Upper Continental Crust (UCC) and Lower Continental Crust (LCC). Data from Saunders and Tarney (1984), Sun (1980), Weaver and Tarney (1984).

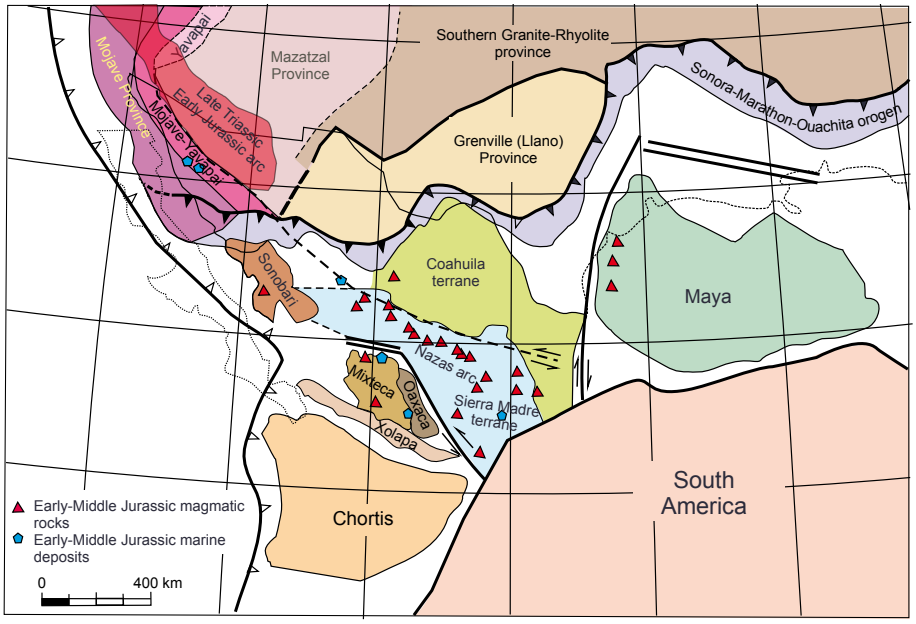

FIGURE 8 | Hypothetical reconstruction of the main crustal blocks for the Early Jurassic time. Laurentian crustal blocks based on Poole *et al.* (2005). Nazas arc magmatism and Jurassic marine deposits based on Godínez-Urban *et al.* (2011).

Paleozoic sandstones from New México was reported (Amato and Mack, 2012; Fig. 9). A possible source for the scarce Neoproterozoic–Middle Cambrian zircons in the SF-05 sample are igneous rocks from Colorado and New México (McMillan and McLemore, 2004), which are interpreted as having formed in an aulacogen located from Colorado to southern Laurentia. An alternative hypothesis is that the Neoproterozoic and Cambrian ages derive from peri-Gondwanan terranes accreted to Laurentia by Late Permian times. Considering that the younger ages in the sample are scarce and disperse, while the Paleo- and Mesoproterozoic ages are prevalent, the southwestern Laurentia origin is preferred as the source of the Francisco Gneiss sediments. Consequently, the Francisco Gneiss sedimentary protolith could have been deposited in a basin located in the southern edge of Laurentia. In this context, the Francisco metasediments would be part of Paleozoic slope and ocean basin sequences that were thrust over coeval shelf sediments in central Sonora at about the Late Permian, forming the fold-and-thrust belt of the Marathon-Ouachita-Sonora orogen of Poole *et al.* (2005).

The comparison of the detrital zircon ages of the Francisco paragneiss with those reported from the Río Fuerte Formation located ~35km east of the study area indicates that important differences exist between these two sequences (Fig. 9), mainly in the size of the respective age clusters. The detrital zircon plots of the Río Fuerte Formation have main peaks suggesting an intra-Iapetus origin with peri-Gondwanan influence (Vega-Granillo *et al.*, 2008, 2011), which are similar to those found in the Ixcamilpa Suite of the Acatlán Complex of southern

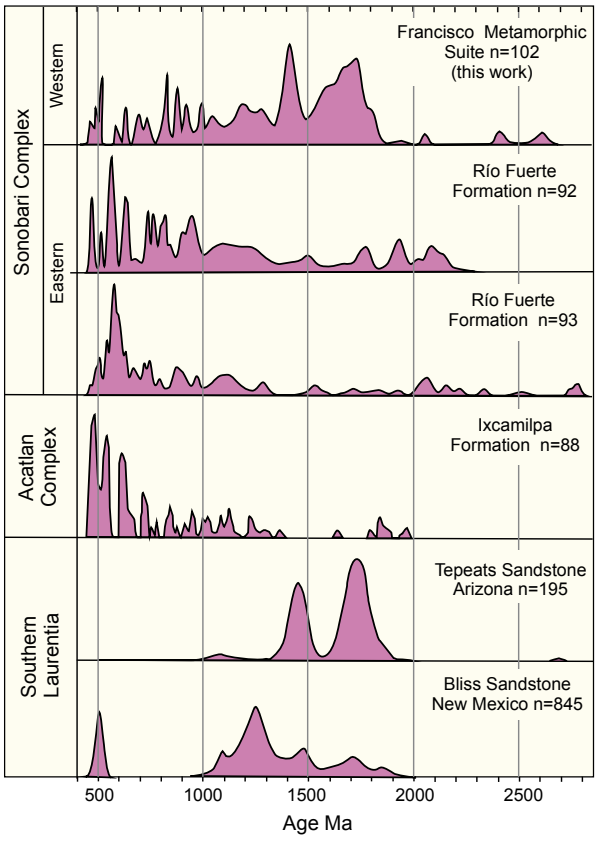

FIGURE 9 | Comparison of the relative probability plots of the Francisco Gneiss with the Río Fuerte Formation (Vega-Granillo *et al.*, 2008), both of the Sonobari Complex, the Ixcamilpa Suite of the Acatlán Complex in southern México (Talavera-Mendoza *et al.*, 2005), and sandstones both from Arizona (Gehrels *et al.*, 2011) and New Mexico (Amato and Mack, 2012) of southern Laurentia.

TABLE 4 | VG5400 Ar-Ar laser step heating experiments SF-45 hornblende large

Pwr	$^{39}Ar \times 10^{-6}$	F ^{39}Ar	$^{40}Ar^*/^{39}Ar_K$	Age in Ma			% $^{40}Ar^*$	$^{40}Ar/^{36}Ar$	$^{37}Ar_{Ca}/^{39}Ar_K$
0.20	2.903	0.0085	67.49 ± 9.57	370.90 ± 47.56	a	‡	24.72	392.53	0.624
0.50	4.422	0.0130	31.07 ± 3.64	180.30 ± 20.07	b	‡	23.06	384.05	2.062
0.80	3.502	0.0103	15.61 ± 4.37	92.83 ± 25.34	c	‡	31.08	428.78	1.458
1.40	23.932	0.0704	8.44 ± 0.66	50.75 ± 3.93	d		41.59	505.90	14.058
2.00	193.252	0.5681	9.78 ± 0.37	58.72 ± 2.19	e		68.61	941.31	13.126
2.60	81.745	0.2403	8.89 ± 0.23	53.44 ± 1.37	f		63.08	800.32	14.834
3.20	12.468	0.0367	---	---	g	‡	---	---	13.761
4.00	17.928	0.0527	8.38 ± 0.65	50.42 ± 3.84	h		94.70	5578.91	17.103

Irradiation parameter J= 0.003382 ± 0.000013 (obtained with sanidine FCT 2 (27.84±0.04Ma), irradiated alongside the samples).

Integrated results

$^{39}Ar \times 10^{-6}$	$^{40}Ar^*/^{39}Ar_K$	Age in Ma	% $^{40}Ar^*$	$^{40}Ar/^{36}Ar$	$^{37}Ar_{Ca}/^{39}Ar_K$
340.2	10.19 ± 0.25	61.10 ± 1.51	55.76	667.91	13.465

‡ fractions ignored in the isochron age calculation.
The integrated results given are not accurate, because the signal of mass 36 could not be evaluated for fraction "g", since this fraction only represents 3.67% of the total ^{39}Ar released, it is not too critical for the interpretation.
The best estimate for the age of this sample is taken from the plateau age, which was calculated with the weighted mean of fractions d to f, yielding t_p = 54.59 ± 3.60Ma, 87.88% of ^{39}Ar released in 3 consecutive fractions, MSWD = 2.58.
An isochron age of t_c = 54.08 ± 9.66Ma, was calculated using fractions d to e and h.
Within errors the plateau and isochron ages are statistically indistinguishable.

México (Fig. 9). On the other side, the main peaks of the Francisco paragneiss are also prominent in lower Paleozoic sequences from southern Laurentia (Fig. 9).

Late Paleozoic-early Mesozoic magmatism

The felsic magmatism of the Francisco Gneiss may be related to the Middle to Late Permian magmatism of northwestern Sonora (Arvizu *et al.*, 2009), even though magmatic rocks of these ages have not been reported from central or southern Sonora. Permian magmatism in Sonora is calc-alkaline with island arc affinity (Arvizu *et al.*, 2009), while felsic magmatism of the Francisco Gneiss is also calc-alkaline (Keppie *et al.*, 2006). Although Keppie *et al.* (2006) favor a continental rift environment for the felsic rocks of the Francisco Gneiss, its geochemical data may be interpreted as indicating a volcanic-arc setting, for example if they are plotted in the Rb-(Y+Nb) discrimination diagram of Pearce *et al.* (1984).

Francisco Gneiss amphibolites

The 67 ± 5Ma $^{40}Ar/^{39}Ar$ age of amphibole from the Francisco amphibolite indicates the time when amphibole temperature falls under its closure temperature of ~500°C for the K-Ar system (Harrison, 1981). The protolith age of the amphibolite remains to be defined, but it must be between the 248 ± 28Ma age of the orthogneiss protolith and the 67 ± 5Ma cooling age of the amphibolite. Considering that the Francisco Gneiss underwent amphibolite facies metamorphism-migmatization, as well as intrusion of the Upper Cretaceous Los Parajes Granodiorite, the Ar-Ar age may reflect cooling after either: i) latest Early Cretaceous orogenic metamorphism, in the case that the rocks remained buried until the Late Cretaceous; ii) Late Cretaceous contact metamorphism, which may cause total resetting of the K-Ar system. The 112 to 98Ma U-Pb titanite ages and the 91 to 51Ma U-Pb ages obtained from the Francisco Gneiss (Keppie *et al.*, 2006) evidence the Late Cretaceous metamorphism. In southern Sinaloa, hornblende K-Ar ages of syntectonic intrusions range between 98 and 90Ma, while post-tectonic intrusions are younger (Henry *et al.*, 2003). Then, the ages of different minerals would reflect the successive times when the respective dating system was closed, first U-Pb in titanite, then U-Pb in xenotime and finally K-Ar in amphibole. On the other hand, widespread epidotization of the Francisco Gneiss may evidence a contact metamorphic event. Also, numerous non-foliated felsic dikes, probably related with Upper Cretaceous granitoids as the Los Parajes granodiorite, traverse the gneisses. Based on the chronological data, the orogenic metamorphism imposed on the Francisco Gneiss rocks may be related to the accretion of the Lower Cretaceous Alisitos arc (Silver and Chapell, 1988) against

northwestern México, which is considered to have been completed at 108 to 105Ma (*e.g.* Alsleben *et al.*, 2008), and subsequent slow exhumation during the Late Cretaceous. However, it cannot be ruled out that a Late Cretaceous contact metamorphism may have altered the Ar-Ar ages in amphibole.

Petrogenesis of mafic Sonobari intrusive rocks

Geochemical features of the pre-collision and post-collision transitional mafic rocks of Sonobari help to establish their genesis. The Francisco Gneiss amphibolites have concentrations similar to N-MORB, which may reflect an asthenospheric upper mantle source type (Hawkesworth and Powell, 1980; Wilson, 1989). The absent or weak depletion of Eu in mafic rocks suggests that plagioclase has not been fractionated between the source and the surface. Also, it suggests that the source area lacked plagioclase, or that plagioclase in the source area was completely melted when basalt was generated (*e.g.* Hearn *et al.*, 1981; Rollinson, 1993). The concentrations of Ti and V in amphibolites and gabbros (Fig. 10A) indicate that these rocks are similar to Middle Oceanic Ridge Basalts (MORB) and Back Arc Basin Basalts (BABB). However, a MORB setting is unlikely from the field relationships, and the high Ta/Yb and Rb/Y ratios, which point to crustal contamination (Pearce, 1983; Pearce *et al.*, 1990). A crustal component can be detected in the amphibolite suite from the high K, Rb, Ba, Th, U, and Pb values in the multi-element diagram (Fig. 7B) and from the high Rb/Yb and K/Yb ratios (Fig. 10B, C). According to the variation in Th/Yb and U/Yb (Fig. 10D, E), the amphibolites display a significant influence of the upper continental crust. These relations suggest that the mafic magmatism of the Francisco Gneiss is related to rifting in a back-arc setting. Once emplaced, these magmatic rocks underwent orogenic metamorphism that may have originated by collision of the Alisitos arc in the latest Early Cretaceous.

The undeformed Macochin Gabbro is younger than the amphibolites of the Francisco Gneiss, and post-dates the collision of the Alisitos arc. This unit displays a larger assimilation of the lower continental crust than the amphibolites (Fig.s 10D, E). Nevertheless, it shares some geochemical resemblance with these rocks, mainly in Ta/Y, Rb/Y ratios, high-field-strength (HFS) and major element concentrations, which indicate that both units may come from a similar mantle source.

Geochemical comparison

Keppie *et al.* (2006) report seven samples from the Francisco Gneiss as a Late Triassic continental rift tholeiite suite. The geochemical characteristics of the amphibolites studied in this paper agree with those reported by these authors (Figs. 6; 7; 10), although the compositional range in this work is wider, because basalts and andesites are included. The mafic rocks of the western Sonobari Complex described here have remarkable chemical differences with those of the eastern Sonobari Complex (Vega-Granillo *et al.*, 2012), indicating that the magmas were not derived from the same mantle source and are not associated with the same tectonic context (Figs. 7; 10).

Late Cretaceous magmatism

After accretion of the Alisitos arc to mainland México, subduction resumed in the western continental margin, producing a Late Cretaceous–early Tertiary (~90–40Ma) continental arc (*e.g.* McDowell and Clabaugh, 1979; Damon *et al.*, 1983a,b; Silver and Chappell, 1988; Kimbrough *et al.*, 2001; McDowell *et al.*, 2001; Henry *et al.*, 2003). The arc includes the Peninsular Ranges Batholith of Baja California to the west and the Sonora-Sinaloa batholiths in the east. Granite, quartz monzonite, and tonalite,

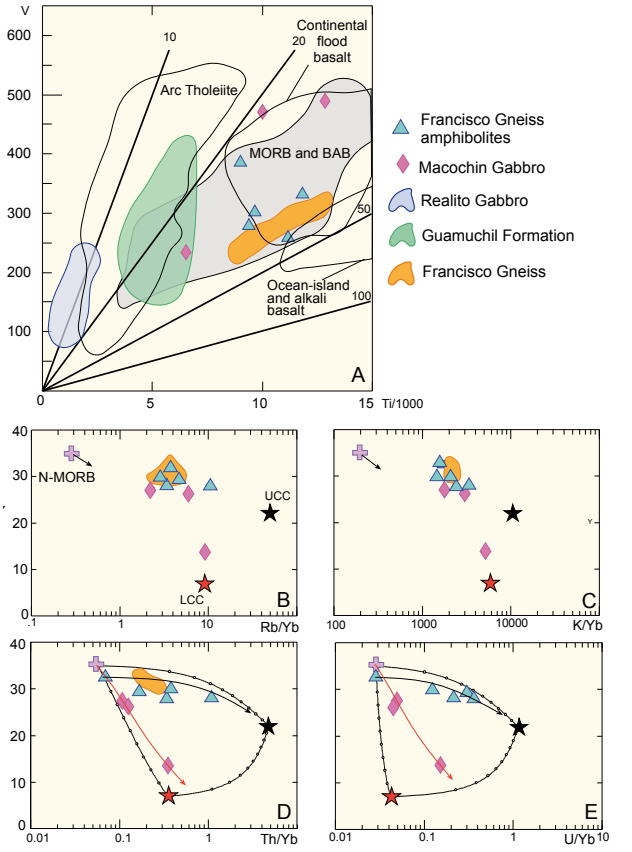

FIGURE 10 | A) V/Ti tectonic discrimination diagram (Shervais, 1982). The Realito Gabbro and Guamuchil Formation data from Vega-Granillo *et al.* (2012); previous Francisco Gneiss data from Keppie *et al.* (2006). B) Y vs. Rb/Yb. C) Y vs. K/Yb. D) Y vs. Th/Yb. E) Y vs. U/Yb. Solid lines represent binary mixing between end members: N-MORB, UCC, and LCC, according the equation by Langmuir et al. (1978). Assimilation trends of the most mafic amphibolite and N-MORB are shown for comparison. See text for discussion.

intruding the metamorphic units in the eastern El Fuerte region, which yield K-Ar biotite cooling ages of 57 ± 1Ma (Damon *et al.*, 1983b), form part of this continental arc. Also, the Los Parajes Granodiorite, intruded at 64 ± 1Ma, and the Macochin Gabbro, cooled at 54 ± 10Ma, should be considered part of this magmatic arc.

CONCLUSIONS

The Francisco Gneiss is composed of sedimentary, igneous felsic, and mafic protoliths. Field relationships suggest that metasedimentary rocks were intruded by granodioritic bodies and subsequently by mafic dikes. Afterwards, these rocks were transformed in paragneisses, orthogneisses and amphibolites, respectively. Detrital zircon ages of metasediment sample SF-05 have main distributions from ca. 500 to ca. 2000Ma, with the main peak at ca. 1690Ma, and scarce older zircons. This distribution suggests that the sediments mainly derived from the Precambrian crust of southwestern Laurentia. The mean age of 509 ± 29Ma from the youngest zircon cluster indicates a Middle Cambrian maximum deposition age.

An upper intercept zircon age of 248 ± 28Ma obtained from the Francisco orthogneiss previously dated as ~220 and ~206Ma (Anderson and Schmidt, 1983; Keppie *et al.*, 2006, respectively) is interpreted as a magmatic age. The age distribution of this rock is biased towards the youngest ages, probably as a result of Pb-loss caused by amphibolite facies metamorphism imprinting the rock. The $^{40}Ar/^{39}Ar$ 67 ± 5Ma age obtained from the Francisco Gneiss amphibolite is a cooling age after either orogenic or contact metamorphism. The amphibolite facies metamorphism overprinting the Francisco Gneiss occurred between the 248 ± 28Ma age of the orthogneiss protolith and the amphibolite cooling age of 67 ± 5Ma. Previous U-Pb age data of titanite and xenotime ranging from 112 to 51Ma (Keppie *et al.*, 2006) suggest that an orogenic metamorphic event occurred during the latest Early Cretaceous and therefore, it may be related to the accretion of the Alisitos arc to northwestern México. The Francisco Gneiss was intruded by the Los Parajes Granodiorite at about 64 ± 1Ma and then by the Macochin Gabbro, the latter yields $^{40}Ar/^{39}Ar$ cooling ages of 54 ± 10Ma and 47 ± 5Ma.

The Francisco amphibolite has similar geochemical composition as olivine- and quartz- tholeiites, with HFS concentrations similar to N-MORB. However, its high Ta/Yb and Rb/Y ratios point to crustal contamination, which is also indicated by high K, Rb, Ba, Th, U, and Pb values. The Ti and V ratios and high concentrations of LFS indicate a tectonic setting similar to BABB. The Macochin Gabbro corresponds to olivine tholeiites, locally with normative nepheline.

ACKNOWLEDGMENTS

The research for this paper was financed by a CONACYT (177668) grant to Ricardo Vega-Granillo. We appreciate the helpful assistance of M.A. García García with the $^{40}Ar/^{39}Ar$ mass spectrometry, A.S. Rosas Montoya, V.M. Pérez Arroyo, and G. Rendón with the $^{40}Ar/^{39}Ar$ sample preparation. We gratefully acknowledge Dante Morán Zenteno and Bodo Weber, whose valuable reviews helped to improve this manuscript.

REFERENCES

Alsleben, H., Wetmore, P.H., Schmidt, K.L., Paterson, S.R., Melis, E.A., 2008. Complex deformation during arc-continent collision: Quantifying finite strain in the accreted Alisitos arc, Peninsular Ranges batholith, Baja California. Journal of Structural Geology, 30, 220-236.

Amato, J., Mack, G.H., 2012. Detrital zircon geochronology from the Cambrian-Ordovician Bliss Sandstone, New México: Evidence for contrasting Grenville-age and Cambrian sources on opposite sides of the Transcontinental Arch. Geological Society of America Bulletin, 124, 1826-1840. doi:10.1130/B30657.1

Amato, J., Boullion, A., Serna, A., Sanders, A., Farmer, G., Gehrels, G., Wooden, J., 2008. Evolution of the Mazatzal province and the timing of the Mazatzal orogeny: Insights from U-Pb geochronology and geochemistry of igneous and metasedimentary rocks in southern New México. Geological Society of America Bulletin, 120(3/4), 328-346.

Andersen T., 2002. Correction of common lead in U–Pb analyses that do not report ^{204}Pb. Chemical Geology, 192, 59-79.

Anderson, T.H., Silver, L.T., 1981. An overview of Precambrian rocks in Sonora. Revista, Instituto de Geologia, Universidad Nacional Autónoma de México (U.N.A.M.), 5(2), 131-139.

Anderson, T.H., Schmidt, V.A., 1983. A model of the evolution of Middle America and the Gulf of México–Caribbean Sea region during Mesozoic time. Geological Society of America Bulletin, 94, 941-966.

Anderson, T.H., Silver, L.T., 2005. The Mojave–Sonora megashear – Field and analytical studies leading to the conception and evolution of the hypothesis. In: Anderson, T.H., Nourse, J.A., McKee, J.W., Steiner, M.B. (eds.). The Mojave–Sonora Megashear Hypothesis: Development, Assessment, and Alternatives. Geological Society of America, 393 (Special Paper), 1-50.

Arvizu, H.E., Iriondo, A., Izaguirre, A., Chávez-Cabello, G., Kamenow, G.D., Solís-Pichardo, G., Foster, D.A., Lozano-Santa Cruz, R., 2009. Rocas graníticas pérmicas en la Sierra Pinta, NW de Sonora, México: Magmatismo de subducción asociado al inicio del margen continental activo del SW de Norteamérica. Revista Mexicana de Ciencias Geológicas, 26(3), 709-728.

Barbeau, D.L.Jr., Ducea, M.N., Gehrels, G.E., Kidder, S., Wetmore, P.H., Saleeby, J.B., 2005. U-Pb detrital-zircon

geochronology of northern Salinian basement and cover rocks. Geological Society of America Bulletin, 117, 466-481.

Campa, U.M.F., Coney, P., 1983. Tectono-stratigraphic terranes and mineral resource distributions of México. Canadian Journal of Earth Sciences, 20, 1040-1051.

Damon, P.E., Clark, K.F., Shafiqullah, M., 1983a. Geochronology of the porphyry copper deposits and related mineralization of México. Canadian Journal of Earth Sciences, 20, 1052-1071.

Damon, P.E., Shafiqullah, M., Roldán-Quintana, J., Cochemé, J.J., 1983b. El batolito Laramide (90–40 Ma) de Sonora. Asociación de Ingenieros de Minas, Metalurgistas y Geólogos de México (AIMMGM), Memoria Técnica XV, Guadalajara, 63-95.

De Cserna, Z., Kent, B.H., 1961. Mapa geológico de reconocimiento y secciones estructurales de la región de San Blas y El Fuerte, Estado de Sinaloa: Cartas Geológicas y Mineras Nº 4, escala 1:100,000, Instituto de Geología, Universidad Nacional Autónoma de México.

Escamilla-Torres, T., Saldaña-Saucedo, G., Polanco-Salas, A., Quevedo-León, A., Moreno-López, M.H., 2000. Carta Geológico-Minera "Huatabampo G12-6" escala 1:250,000.

Gehrels, G.E., Stewart, J.H., 1998. Detrital zircon U-Pb geochronology of Cambrian to Triassic miogeosynclinal and eugeosynclinal strata of Sonora, México. Journal of Geophysical Research, B, Solid Earth and Planets, 103(2), 2471-2487.

Gehrels, G.E., Blakey, R., Karlstrom, K.E., Timmons, J.M., Dickinson, B., Pecha, M., 2011. Detrital zircon U-Pb geochronology of Paleozoic strata in the Grand Canyon, Arizona. Lithosphere, 3, 183-200.

Godínez-Urban, A., Lawton, T.F., Molina-Garza, R.S., Iridondo, A., Weber, B., López-Martínez, M., 2011. Jurassic volcanic and sedimentary rocks of the La Silla and Todos Santos Formations, Chiapas: Record of Nazas arc magmatism and rift-basin formation prior to opening of the Gulf of México. Geosphere, 7(1), 121-144.

González-León, C.M., Valencia, V.A., Lawton, T.F., Amato, J.M., Gehrels, G.E., Leggett, W.J., Montijo-Contreras, O., Fernández, M.A., 2009, The lower Mesozoic record of detrital zircon U-Pb geochronology of Sonora, México, and its paleogeographic implications. Revista Mexicana de Ciencias Geológicas, 26, 301-314.

Gross, E.L., Stewart, J.H., Gehrels, G.E., 2000. Detrital zircon geochronology of Neoproterozoic to Middle Cambrian miogeoclinal and platformal strata: northwest Sonora, México. Geofísica Internacional, 39, 295-308.

Harrison, T.M., 1981. Diffusion of ^{40}Ar in hornblende. Contributions to Mineralogy and Petrology, 70, 324-331.

Hawkesworth, J., Powell C., 1980. Magma genesis in the Lesser Antilles island arc. Earth Planetary Science Letters, 51, 297-308.

Hearn, B.C.Jr., Donelly-Nolan, J.M., Goff, F.E., 1981. The Clear Lake Volcanics: Tectonic setting and magma sources. Research in the Geysers-Clear Lake Geothermal Area, Northern California. In U.S. Geological survey, 1141 (Professional Paper), 25-46.

Henry, C.D., McDowell, F.W., Silver, L.T., 2003. Geology and geochronology of granitic batholitic complex, Sinaloa, México: implications for Cordilleran magmatism and tectonics. Geological Society of America, 374 (Special Paper), 237-273.

Hoskin, P., Schaltegger, U., 2003. The composition of zircon and igneous and metamorphic petrogenesis. In: Hanchar, J., Hoskin, P. (eds.). Zircon, Reviews in Mineralogy and Geochemistry, 53, 27-62.

Irvine, T.N., Baragar, W.R.A., 1971. A guide to the chemical classification of the common volcanic rocks. Canadian Journal of Earth Sciences, 8, 523-548.

Karlstrom, K.E., Humphreys, G., 1998. Influence of Proterozoic accretionary boundaries in the tectonic evolution of western North America: Interaction of cratonic grain and mantle modification events. Rocky Mountain Geology, 33, 161-179.

Keppie, D.J., Dostal, J., Miller, B.V., Ortega-Rivera, A., Roldán-Quintana, J., Lee, J.W.K., 2006. Geochronology and geochemistry of the Francisco Gneiss: Triassic continental rift tholeiites on the Mexican margin of Pangea metamorphosed and exhumed in a Tertiary core complex. International Geology Review, 48(1), 1-16.

Kimbrough, D.L., Smith, D.P., Mahoney, J.B., Grove, M., Gastil, R.G., Ortega-Rivera, A., 2001. Forearc-basin sedimentary response to rapid Late Cretaceous batholith emplacement in the Peninsular Ranges of southern and Baja California. Geology, 29(6), 491-494.

Langmuir, C.H., Vocke, R.D., Hanson, G.N., 1978. A general mixing equation with applications to Icelandic basalts. Earth and Planetary Science Letters, 37, 380-392.

Ludwig, K.L., 2008. Isoplot 3.70. A geochronological toolkit for Microsoft Excel. Berkeley Geochronology Center, 4 (Special Publications), 1-77.

Marshall, D.J., 1988. Cathodoluminescence of geological materials. Boston, Sydney, Wellington, Unwin Hyman, 146pp.

Maurel, O., Monié, P., Respaut, J.P., Leyreloup, A.F., Maluski, H., 2003. Pre-metamorphic $^{40}Ar/^{39}Ar$ and U–Pb ages in HP metagranitoids from the Hercynian belt (France). Chemical Geology, 193, 195-214.

McDonough, W.F., Sun, S.S., 1995. Composition of the Earth. Chemical Geology, 120, 223-253.

McDowell, F.W., Clabaugh, S.E., 1979. Ignimbrites of the Sierra Madre Occidental and their relation to the tectonic history of western México. In: Chapin, E.C., Elston, W.E. (eds.). Ash-flow tuffs. Geological Society of America, 180 (Special Paper), 113-124.

McDowell, F.W., Roldán-Quintana, J., Connelly, J.N., 2001. Duration of Late Cretaceous–early Tertiary magmatism in east-central Sonora, México. Geological Society of America Bulletin, 113(4), 521-531.

McMillan, N.J., McLemore, V.T., 2004. Cambrian–Ordovician magmatism and extension in New México and Colorado. New México Bureau of Geology & Mineral Resources Bulletin, 160, 1-11.

Middlemost, E.A.K., 1994. Naming materials in magma/igneous rock system. Earth Science Reviews, 37, 215-224.

Miyashiro, A., 1974. Volcanic rocks series in island arcs and active continental margins. American Journal of Sciences, 274, 321-355.

Miyashiro, A., 1978. Nature of alkalic volcanic rock series. Contributions to Mineralogy and Petrology, 66, 91-104.

Mullan, H.S., 1978. Evolution of the Nevadan orogen in northwestern México. Geological Society of America Bulletin, 89(8), 1175-1188.

Mullan, H.S., Bussell, M.A., 1977. The basic rocks series in batholithic associations: Geological Magazine, 114, 265-280.

Pearce, J.A., 1983. Role of the sub-continental lithosphere in magma genesis at active continental margins. In: Hawkesworth, C.J., Norry, M.J. (eds.). Continental Basalts and Mantle Xenoliths, Nantwich, Cheshire, United Kingdom. Cambridge, Shiva Publications, 230-250.

Pearce, J.A., 1996. A user's guide to basalt discrimination diagrams. In: Wyman, D.A. (ed.). Trace element geochemistry of volcanic rocks: Applications for massive sulphide exploration. Geological Association of Canada, Short Course Notes, 12, 79-113.

Pearce, J.A., Harris, N.B.W., Tindle, A.G., 1984, Trace element discrimination diagrams for the tectonic interpretation of granitic rocks. Journal of Petrology, 25, 956-983.

Pearce, J.A., Bender, J.F., De Long, S.E., Kidd, W.S.F., Low, P.J., Guner, Y., Saroglu, F., Yilmaz, Y., Moorbath, S., Mitchell, J.G., 1990. Genesis of collision volcanism in Eastern Anatolia, Turkey. Journal of Volcanology and Geothermal Research, 44, 189-229.

Peiffer-Rangin, F., 1979. Les zones isopiques du Paléozoique inférieur du NW Mexicain. Temoins du relais entre les Appalaches et la cordillère ouest-américaine. Paris, Comptes Rendus Académie Sciences, série D, 288, 1517-1519.

Poole, F.G., Perry, W.J.Jr., Madrid, R.J., Amaya-Martínez, R., 2005. Tectonic synthesis of the Ouachita–Marathon–Sonora orogenic margin of southern Laurentia: Stratigraphic and structural implications for timing of deformational events and plate-tectonic model. In: Anderson, T.H., Nourse, J.A., McKee, J.W., Steiner, M.B. (eds.). The Mojave–Sonora Megashear Hypothesis: Development, Assessment, and Alternatives. Geological Society of America, 393 (Special Paper), 543-596.

Reese, J.F., Mosher, S., Connelly, J., Roback, R., 2000. Mesoproterozoic chronostratigraphy of the southeastern Llano uplift, central Texas. Geological Society of America Bulletin, 112, 278-291.

Rollinson, H.R., 1993. Using geochemical data: evaluation, presentation, interpretation. Pearson-Prentice Hall, 352pp.

Saunders, A.D., Tarney, J., 1984. Geochemical characteristics of basaltic volcanism within back-arc basins. In: Kokelaar, B.P., Howells, M.F. (eds.). Marginal basin geology. London, Geological Society, 16 (Special Publications), 59-76.

Sedlock, R.L., Ortega, G.F., Speed, R.C., 1993. Tectono-stratigraphic Terranes and Tectonic Evolution of México. Geological Society of America, 278 (Special Paper), 153pp.

Shervais, J.W., 1982. Ti-V plots and petrogenesis of modern and ophiolitic lavas. Earth and Planetary Science Letters, 59, 101-118.

Silver, L.T., Chappell, B.W., 1988. The Peninsular Ranges Batholith: an insight into the evolution of the Cordilleran batholiths of southwestern North America. Transactions of the Royal Society of Edinburgh, Earth Sciences, 79, 150-121.

Sláma, J., Košler, J., Condon, D.J., Crowley, J.L., Gerdes, A., Hanchar, J.M., Horstwood, M.S.A., Morris, G.A., Nasdala, L., Norberg, N., Schaltegger, U., Schoene, B., Tubrett, M.N., Whitehouse, M.J., 2008. Plešovice zircon – A new natural reference material for U-Pb and Hf isotopic microanalysis. Chemical Geology, 249, 1-35.

Solari, L., Tanner, M., 2011. U-Pb age, a fast data reduction script for LA-ICP-MS U-Pb geochronology. Revista Mexicana de Ciencias Geológicas, 28(1), 83-91.

Solari, L.A., Torres de León, R., Hernández-Pineda, G., Solé, J., Henández-Treviño, T., Solis, G., 2007. Tectonic significance of Cretaceous-Tertiary magmatic and structural evolution of the northern margin of the Xolapa Complex, Tierra Colorada area, southern México. Geological Society of America Bulletin, 119, 1265-1279.

Solari, L.A., Gómez-Tuena, A., Bernal, J.P., Pérez-Arvizu, O., Tanner, M., 2010. U-Pb zircon geochronology by an integrated LA-ICPMS microanalytical workstation: achievements in precision and accuracy. Geostandards and Geoanalytical Research, 34(1), 5-18.

Steiger R. H., Jäger E., 1977. Subcommission on Geochronology: Convention on the use of decay constants in Geo and Cosmochronology. Earth and Planetary Sciences Letters, 36, 359-362.

Stewart, J.H., Gehrels, G., Barth, A.P., Link, P.K., Christie-Blick, N., Wrucke, C.T., 2001. Detrital zircon provenance of Mesoproterozoic to Cambrian arenites in the western United States and northwestern México. Geological Society of America Bulletin, 113(10), 1343-1356.

Sun, S.S., 1980. Lead isotopic study of young volcanic rocks from mid-ocean ridges, ocean islands and island arcs. Philosophical Transactions Royal Society, A297, 409-445.

Sun, S.S., McDonough, W.F., 1989. Chemical and isotopic systematic of oceanic basalts: implications for mantle compositional processes. In: Saunders, A.D., Norry, M.J. (eds.). Magmatism in Ocean Basins. Geological Society of London, 42 (Special Publication), 313-345.

Talavera-Mendoza, O., Ruíz, J., Gehrels, G.E., Meza-Figueroa, D.M., Vega-Granillo, R., Campa-Uranga, M.F., 2005. U–Pb geochronology of the Acatlán Complex and implications for the Paleozoic paleogeography and tectonic evolution of southern México. Earth and Planetary Science Letters, 235(3-4), 682-699.

Thompson, R.N., 1984. Dispatches from the basalt front. 1. Experiments. Proceedings Geological Association, 95, 249-262.

Van Schmus, W.R., Bickford, M.E., Turek, E., 1996. Proterozoic geology of the east-central mid-continent basement. In: van

der Pluijm, B.A., Catacosinos, P.A. (eds.). Basement and basins of eastern North America. Geological Society of America, 308 (Special Paper), 7-32.

Vega-Granillo, R., Salgado-Souto, S., Herrera-Urbina, S., Valencia, V., Ruiz, J., Meza-Figueroa, D., Talavera-Mendoza, O., 2008. U-Pb detrital zircon data of the Rio Fuerte Formation (NW México): its peri-Gondwanan provenance and exotic nature in relation to southwestern North America. Journal South American Earth Sciences, 26, 343-354.

Vega-Granillo, R., Salgado-Souto, S., Herrera-Urbina, S., Valencia-Gómez, V., Vidal-Solano, J.R., 2011. Metamorphism and deformation in the El Fuerte region: their role in the tectonic evolution of NW México. Revista Mexicana de Ciencias Geológicas, 28(1), 10-23.

Vega-Granillo, R., Vidal-Solano, J., Herrera-Urbina, S., 2012. Island arc tholeiites of Early Silurian, Late Jurassic and Late Cretaceous ages in the El Fuerte region, northwestern México. Revista Mexicana de Ciencias Geológicas, 29(2), 492-513.

Weaver, B., Tarney, J., 1984. Empirical approach to estimating the composition of the continental crust. Nature, 310, 575-557.

Whitmeyer, S.J., Karlstrom, K.E., 2007. Tectonic model for the Proterozoic growth of North America. Geosphere, 3(4), 220-259.

Wilson, M., 1989. Igneous Petrogenesis. Dordrecht (The Netherlands), Springer, 466pp.

Winchester, J.A., Floyd, P.A., 1977. Geochemical discrimination of different magma series and their differentiation products using immobile elements. Chemical Geology, 20, 325-342.

Windley, B.F., 1993. Proterozoic anorogenic magmatism and its orogenic connection. Journal of the Geological Society London, 150, 39-50.

York, D., Evensen, N.M., López-Martínez, M., De Basabe-Delgado, J., 2004. Unified equations for the slope, intercept, and standard errors of the best straight line. American Journal of Physics, 73, 367-375.

Manuscript received September 2012;
revision accepted October 2013;
published Online November 2013.

ELECTRONIC APPENDIX

TABLE I | U-Pb geochronologic data

				CORRECTED RATIOS											CORRECTED AGES (Ma)					
Zircon	U(ppm)	Th(ppm)	Th/U	$^{207}Pb/^{206}Pb$	±1σ	$^{207}Pb/^{235}U$	±1σ	$^{206}Pb/^{238}U$	±1σ	$^{208}Pb/^{232}Th$	±1σ	Rho	$^{206}Pb/^{238}U$	±1σ	$^{207}Pb/^{235}U$	±1σ	$^{207}Pb/^{206}Pb$	±1σ	Best age (Ma)	±1σ
SF-12																				
1	312	191	0.61	0.05173	0.00078	0.23392	0.00381	0.03283	0.00021	0.00968	0.00013	0.38	208	1	213	3	273	33	208	1
2	320	71	0.22	0.05253	0.00095	0.16054	0.00308	0.02224	0.00015	0.00948	0.00018	0.33	141.8	0.9	151	3	309	39	~~142~~	~~1~~
3	393	128	0.33	0.04936	0.00079	0.20027	0.00338	0.02947	0.00016	0.00937	0.00012	0.32	187	1	185	3	165	35	187	1
4	487	167	0.34	0.051	0.00066	0.22888	0.00342	0.03264	0.00024	0.00984	0.00018	0.5	207	1	209	3	241	28	207	1
5	279	144	0.51	0.05196	0.00094	0.24009	0.0045	0.03353	0.00017	0.01002	0.00013	0.26	213	1	218	4	284	39	213	1
6	312	120	0.38	0.05275	0.00079	0.20908	0.00336	0.02883	0.00016	0.00993	0.00018	0.36	183	1	193	3	318	34	183	1
7	382	261	0.68	0.04999	0.0008	0.23044	0.00391	0.03351	0.00019	0.01005	0.00012	0.33	212	1	211	3	195	37	212	1
8	175	123	0.70	0.05071	0.00112	0.23223	0.00538	0.03336	0.00024	0.00953	0.00012	0.3	212	1	212	4	228	50	212	1
9	330	135	0.41	0.05081	0.00091	0.21244	0.00398	0.03036	0.00016	0.00997	0.00013	0.29	193	1	196	3	232	41	193	1
	278	4	0.01	0.05141	0.00118	0.10181	0.00246	0.01442	0.00011	0.01713	0.00154	0.31	92.3	0.7	98	2	259	50	~~92~~	~~1~~
11	404	194	0.48	0.05144	0.00067	0.22788	0.00323	0.03221	0.00018	0.00969	0.00012	0.39	204	1	208	3	261	28	204	1
12	524	281	0.54	0.05057	0.00066	0.22086	0.00311	0.0317	0.00017	0.00972	0.00012	0.38	201	1	203	3	221	29	201	1
13	173	82	0.47	0.05023	0.001	0.23436	0.00488	0.03401	0.0002	0.01031	0.00015	0.29	216	1	214	4	206	44	216	1
14	376	98	0.26	0.05009	0.00103	0.18017	0.00396	0.02609	0.00014	0.00823	0.00005	0.33	166	0.9	168	3	199	45	~~166~~	~~1~~
15	324	155	0.48	0.0523	0.00078	0.23429	0.00375	0.03262	0.00018	0.00997	0.00013	0.36	207	1	214	3	299	32	207	1
16	190	75	0.39	0.05086	0.00112	0.22434	0.00542	0.03218	0.00032	0.00937	0.00014	0.41	204	2	206	4	234	48	204	2
17	237	86	0.36	0.05103	0.0011	0.20357	0.00472	0.02893	0.00016	0.00911	0.00005	0.29	184	1	188	4	242	47	184	1
18	440	110	0.25	0.05068	0.00071	0.22001	0.00333	0.03157	0.00018	0.00958	0.00015	0.38	200	1	202	3	226	31	200	1
19	279	184	0.66	0.0539	0.00097	0.2499	0.00471	0.03364	0.00019	0.01029	0.00013	0.3	213	1	226	4	367	38	213	1
20	316	128	0.40	0.0519	0.00088	0.21889	0.00396	0.03068	0.00019	0.00959	0.00016	0.35	195	1	201	3	281	37	195	1
21	374	150	0.40	0.05099	0.00082	0.21217	0.00369	0.03026	0.00021	0.00959	0.00013	0.38	192	1	195	3	240	35	192	1
22	309	158	0.51	0.04961	0.00074	0.22768	0.00367	0.03341	0.0002	0.00998	0.00014	0.38	212	1	208	3	177	33	212	1
23	212	96	0.45	0.05231	0.00105	0.23168	0.00494	0.03221	0.00024	0.00978	0.00015	0.34	204	1	212	4	299	43	204	1
24	225	62	0.27	0.05175	0.00123	0.21474	0.0055	0.0301	0.00017	0.00946	0.00005	0.25	191	1	198	5	274	54	191	1
25	567	251	0.44	0.05092	0.00071	0.20838	0.00325	0.02971	0.0002	0.00938	0.00011	0.45	189	1	192	3	237	30	189	1
26	326	64	0.20	0.05092	0.00092	0.20235	0.00591	0.0291	0.00067	0.00906	0.00024	0.79	185	4	187	5	237	39	~~185~~	~~4~~
27	241	99	0.41	0.0511	0.00102	0.23822	0.00498	0.03388	0.00021	0.01056	0.00017	0.3	215	1	217	4	245	43	215	1
28	255	77	0.30	0.05294	0.00079	0.21241	0.00367	0.02919	0.00025	0.0103	0.00016	0.5	185	2	196	3	326	32	185	2
29	250	97	0.39	0.05387	0.00086	0.24687	0.00416	0.03327	0.00018	0.00998	0.00015	0.32	211	1	224	3	366	34	211	1
30	333	141	0.42	0.05398	0.00103	0.21742	0.00434	0.02934	0.00018	0.00935	0.00013	0.29	186	1	200	4	370	41	186	1
31	361	224	0.62	0.05049	0.00106	0.19871	0.00436	0.02857	0.00018	0.00908	0.00011	0.29	182	1	184	4	218	46	182	1
32	219	85	0.39	0.05098	0.00097	0.22524	0.00447	0.03216	0.00018	0.00964	0.00014	0.28	204	1	206	4	240	41	204	1
33	529	78	0.15	0.0517	0.00088	0.19922	0.00357	0.02807	0.00016	0.00972	0.00017	0.31	178	1	184	3	272	37	~~178~~	~~1~~
34	324	197	0.61	0.05153	0.00077	0.21932	0.00356	0.03097	0.00019	0.00943	0.00013	0.39	197	1	201	3	265	32	197	1
35	216	84	0.39	0.05155	0.00108	0.22436	0.00487	0.03159	0.00017	0.00991	0.00017	0.26	200	1	206	4	266	45	200	1
36	347	211	0.61	0.05224	0.00084	0.23325	0.00397	0.03247	0.00019	0.00992	0.00012	0.33	206	1	213	3	296	35	206	1
37	631	353	0.56	0.0506	0.00066	0.21212	0.00318	0.03044	0.00023	0.00967	0.00013	0.49	193	1	195	3	223	28	193	1
38	255	102	0.40	0.05723	0.00235	0.22054	0.00936	0.0286	0.00031	0.01112	0.00061	0.25	182	2	202	8	500	85	182	2
39	331	187	0.57	0.05015	0.0009	0.22907	0.00434	0.03319	0.0002	0.00983	0.00014	0.32	210	1	209	4	202	39	210	1
40	240	46	0.19	0.05571	0.00134	0.163	0.00411	0.02124	0.00017	0.0108	0.00026	0.3	135	1	153	4	441	50	~~135~~	~~1~~
41	2094	6923	3.31	0.05609	0.00067	0.13277	0.00235	0.01714	0.00022	0.00314	0.00015	0.74	110	1	127	2	456	26	~~110~~	~~1~~
42	388	148	0.38	0.05179	0.00078	0.19603	0.00319	0.0275	0.00017	0.00948	0.00012	0.38	175	1	182	3	276	33	~~175~~	~~1~~
43	506	283	0.56	0.05096	0.00087	0.21708	0.00428	0.03094	0.00031	0.00966	0.00039	0.5	196	2	199	4	239	37	196	2
44	345	167	0.48	0.05243	0.00079	0.22973	0.00374	0.03184	0.0002	0.00992	0.00012	0.38	202	1	210	3	304	32	202	1
45	232	147	0.63	0.05099	0.00082	0.23006	0.00394	0.03279	0.0002	0.00954	0.00012	0.34	208	1	210	3	240	35	208	1
46	2852	883	0.31	0.05098	0.00041	0.21343	0.00252	0.03043	0.00026	0.00986	0.00033	0.73	193	2	196	2	240	18	193	2
47	1320	815	0.62	0.05077	0.00056	0.19297	0.00229	0.02763	0.00012	0.00938	0.0001	0.37	175.7	0.8	179	2	230	24	~~176~~	~~1~~
48	355	227	0.64	0.0516	0.00077	0.23407	0.00376	0.03301	0.00019	0.01029	0.00012	0.37	209	1	214	3	268	32	209	1
49	277	120	0.43	0.05267	0.001	0.22784	0.00453	0.03141	0.00018	0.01009	0.00016	0.3	199	1	208	4	315	43	199	1
50	408	260	0.64	0.05147	0.00087	0.21002	0.00377	0.0297	0.00017	0.00982	0.00012	0.34	189	1	194	3	262	38	189	1
51	427	272	0.64	0.0511	0.00072	0.21353	0.00321	0.03041	0.00017	0.0097	0.00012	0.35	193	1	197	3	245	32	193	1
52	263	129	0.49	0.05068	0.00081	0.23078	0.004	0.03308	0.00022	0.01079	0.00015	0.39	210	1	211	3	226	37	210	1
53	323	119	0.37	0.05116	0.00092	0.17263	0.00327	0.02455	0.00014	0.00986	0.00014	0.31	156.3	0.9	162	3	248	41	~~156~~	~~1~~
54	387	213	0.55	0.05128	0.00077	0.21005	0.00336	0.02978	0.00016	0.00944	0.00011	0.34	189	1	194	3	253	34	189	1
55	1055	239	0.23	0.051	0.00066	0.17191	0.00241	0.02451	0.00013	0.00782	0.0001	0.38	156.1	0.8	161	2	241	29	~~156~~	~~1~~
56	367	287	0.78	0.05325	0.00075	0.23037	0.00342	0.03147	0.00016	0.00996	0.00012	0.32	199.7	1	211	3	339	32	200	1
57	335	134	0.40	0.05166	0.00077	0.2064	0.00341	0.02901	0.0002	0.00996	0.00014	0.43	184	1	191	3	270	34	184	1
58	684	258	0.38	0.04837	0.00058	0.2026	0.00274	0.03046	0.00019	0.00952	0.00011	0.46	193	1	187	2	117	28	193	1
SF-51																				
1	151	56	0.37	0.0547	0.00279	0.07579	0.00395	0.01015	0.00011	0.00334	0.00011	0.21	65.1	0.7	74	4	400	116	65	1
2	76	45	0.59	0.05667	0.0038	0.07862	0.00538	0.01027	0.00014	0.00303	0.00008	0.2	65.9	0.9	77	5	479	152	66	1
3	101	40	0.40	0.05472	0.00376	0.07521	0.00542	0.00997	0.00012	0.00311	0.00005	0.21	63.9	0.8	74	5	401	158	64	1
4	74	37	0.51	0.04894	0.00554	0.06948	0.00831	0.0103	0.00018	0.00326	0.00027	0.24	66	1	68	8	145	251	66	1
5	115	77	0.67	0.05632	0.00456	0.07818	0.00641	0.01026	0.00013	0.00299	0.00013	0.16	65.8	0.8	76	6	465	185	66	1
6	65	35	0.54	0.06821	0.00423	0.09804	0.00625	0.01046	0.00016	0.00324	0.00014	0.23	67	1	95	6	875	132	67	1
7	160	88	0.55	0.0466	0.00228	0.06403	0.0032	0.00997	0.0001	0.00289	0.00007	0.2	64	0.6	63	3	29	106	64	1
8	121	79	0.65	0.05618	0.00287	0.0798	0.00413	0.01029	0.00009	0.00319	0.00008	0.16	66	0.6	78	4	459	116	66	1
9	45	23	0.52	0.07519	0.00594	0.11213	0.00911	0.01086	0.00021	0.00345	0.00015	0.23	70	1	108	8	1074	164	70	1
10	154	93	0.60	0.05082	0.00203	0.07028	0.00289	0.01008	0.0001	0.00301	0.00008	0.24	64.7	0.6	69	3	233	92	65	1
11	115	77	0.67	0.05889	0.00277	0.08126	0.00394	0.01005	0.00012	0.00308	0.00008	0.24	64.5	0.8	79	4	563	104	65	1
12	94	45	0.48	0.06099	0.00299	0.08576	0.00433	0.01028	0.00012	0.00321	0.00009	0.24	65.9	0.8	84	4	639	107	66	1
13	120	82	0.68	0.05598	0.00369	0.07655	0.00514	0.01015	0.00012	0.00304	0.00008	0.19	65.1	0.8	75	5	452	150	65	1
14	134	87	0.65	0.04601	0.00235	0.06395	0.00332	0.01014	0.00009	0.00307	0.00008	0.18	65	0.6	63	3	-2	106	65	1
15	136	82	0.60	0.05289	0.00185	0.0734	0.00265	0.01013	0.00009	0.00318	0.00007	0.25	65	0.6	72	3	324	80	65	1
16	96	62	0.64	0.05881	0.00306	0.08648	0.00464	0.01064	0.00014	0.00326	0.0001	0.24	68.2	0.9	84	4	560	116	68	1
17	179	101	0.57	0.05248	0.00189	0.07282	0.0027	0.0101	0.00009	0.00305	0.00006	0.24	64.8	0.6	71	3	306	82	65	1
18	48	25	0.52	0.0698	0.00475	0.10183	0.00716	0.01078	0.00019	0.00393	0.00043	0.25	69	1	98	7	922	144	69	1
19	203	71	0.35	0.04992	0.0019	0.07081	0.0028	0.0103	0.00011	0.00311	0.0001	0.27	66.1	0.7	69	3	191	88	66	1
20	93	43	0.46	0.05809	0.00308	0.08268	0.00449	0.0104	0.00012	0.00344	0.00025	0.22	66.7	0.8	81	4	533	118	67	1
21	118	76	0.65	0.05041	0.00232	0.06956	0.00334	0.01009	0.00014	0.00315	0.00007	0.29	64.7	0.9	68	3	214	108	65	1
22	77	45	0.58	0.05703	0.00342	0.08278	0.00514	0.01067	0.00017	0.00305	0.00014	0.26	68	1	81	5	493	136	68	1
23	55	25	0.45	0.06773	0.00745	0.09279	0.01041	0.00997	0.00022	0.00307	0.00023	0.2	64	1	90	10	860	238	64	1
24	63	39	0.62	0.05076	0.00371	0.07389	0.00556	0.01061	0.00019	0.00301	0.00013	0.24	68	1	72	5	230	168	68	1
25	80	42	0.52	0.06058	0.00309	0.08672	0.00459	0.01045	0.00015	0.00352	0.00013	0.27	67	1	84	4	624	113	67	1
26	79	49	0.62	0.05469	0.00416	0.07847	0.00641	0.01041	0.00016	0.00325	0.00006	0.21	67	1	77	6	400	175	67	1
27	206	103	0.50	0.05153	0.00175	0.07244	0.00256	0.01024	0.0001	0.00307	0.00008	0.28	65.7	0.6	71	2	265	80	66	1
28	94	58	0.62	0.05481	0.00307	0.07806	0.00449	0.01054	0.00014	0.00332	0.0001	0.23	67.6	0.9	76	4	404	129	68	1
29	71	47	0.65	0.06919	0.00581	0.09886	0.00842	0.01047	0.00015	0.0033	0.00012	0.17	67.1	1	96	8	904	179	67	1
30	100	59	0.59	0.05548	0.00261	0.07561	0.00373	0.01004	0.00015	0.00305	0.00011	0.3	64.4	1	74	4	432	107	64	1
31	146	90	0.62	0.05386	0.00189	0.07516	0.00276	0.01011	0.00011	0.00314	0.00008	0.29	64.8	0.7	74	3	365	81	65	1
32	95	63	0.67	0.05769	0.00398	0.08029	0.00564	0.01015	0.00013	0.0032	0.00012	0.19	65.1	0.8	78	5	518	137	65	1
SF-5																				
30	233	185	0.89	0.17415	0.00225	10.08863	0.16756	0.42014	0.00277	0.11611	0.00073	0.5	2261	13	2443	15	2598	21	2598	21
86	48	16	0.33	0.1736	0.0036	9.89	0.13	0.4148	0.0065	0.1151	0.00095	0.01	2237	35	2431	32	2592	53	2592	53
64	223	88	0.40	0.15877	0.0035	9.053	0.14	0.418	0.0065	0.1153	0.0015	0.45	2251	35	2343	36	2442	54	2442	54
34	566	148	0.27	0.15491	0.00155	8.2306	0.10703	0.38535	0.00284	0.1077	0.0008	0.59	2101	13	2257	12	2401	16	2401	16
52	231	193	0.41	0.12635	0.0012	6.2479	0.07088	0.35879	0.00222	0.1042	0.00167	0.55	1976	11	2011	10	2048	16	2048	16
50	351	145	0.67	0.11041	0.00121	4.8933	0.06062	0.32166	0.00183	0.09732	0.00156	0.47	1798	9	1801	10	1806	20	1806	20

TABLE I | Continued

				CORRECTED RATIOS												CORRECTED AGES (Ma)					
Zircon	U(ppm)	Th(ppm)	Th/U	$^{207}Pb/^{206}Pb$	±1σ	$^{207}Pb/^{235}U$	±1σ	$^{206}Pb/^{238}U$	±1σ	$^{208}Pb/^{232}Th$	±1σ	Rho	$^{206}Pb/^{238}U$	±1σ	$^{207}Pb/^{235}U$	Zircon	U(ppm)	Th(ppm)	T	
82	238	91	0.37	0.10975	0.0023	4.331	0.06	0.2906	0.0045	0.0848	0.00165	0.67	1644	25	1699.1	24	1795	37	1795	37
51	171	122	0.77	0.10901	0.0012	3.2062	0.0408	0.2134	0.00137	0.09022	0.00144	0.5	1247	7	1459	10	1783	20	1783	20
98	256	134	0.55	0.1084	0.0022	4.132	0.06	0.2793	0.00405	0.07995	0.00075	0.44	1587.7	23	1660	24	1773	36	1773	36
67	378	121	0.34	0.10734	0.0023	4.127	0.06	0.2834	0.0043	0.0805	0.0014	0.57	1608	24	1659.5	24	1755	37	1755	37
19	69	121	0.32	0.10705	0.00102	4.4208	0.04726	0.29964	0.00147	0.08143	0.00155	0.45	1690	7	1716	9	1750	16	1750	16
58	247	92	0.43	0.10698	0.0023	4.265	0.065	0.2906	0.00435	0.0822	0.0013	0.58	1645	25	1688	26	1748	37	1748	37
12	415	124	0.06	0.10616	0.00099	3.5637	0.03637	0.2438	0.00102	0.07104	0.00114	0.41	1406	5	1541	8	1734	17	1734	17
40	289	25	0.43	0.10607	0.00103	4.1977	0.04404	0.28712	0.00115	0.079	0.0015	0.38	1627	6	1674	9	1733	17	1733	17
33	269	235	0.24	0.10586	0.00101	4.115	0.04517	0.28215	0.00155	0.07175	0.00187	0.49	1602	8	1657	9	1729	17	1729	17
25	512	191	0.13	0.10529	0.00105	4.3648	0.04842	0.30082	0.00144	0.0851	0.00153	0.44	1695	7	1706	9	1719	17	1719	17
60	325	97	0.33	0.10458	0.0021	3.984	0.055	0.2756	0.0041	0.079	0.001	0.44	1569.2	23	1630.8	23	1707	35	1707	35
106	282	70	0.25	0.1046	0.0021	3.878	0.049	0.2692	0.00415	0.0783	0.0011	0.66	1537	24	1609	20	1707	34	1707	34
1	132	46	0.32	0.10436	0.00104	4.3471	0.04841	0.30216	0.00148	0.08588	0.00146	0.45	1702	7	1702	9	1703	18	1703	18
13	866	52	0.35	0.104	0.00103	4.0793	0.0466	0.28452	0.00162	0.08307	0.00133	0.5	1614	8	1650	9	1697	17	1697	17
81	134	34	0.22	0.104	0.0023	3.75	0.055	0.2665	0.00445	0.0812	0.00295	0.69	1523	25	1582	23	1695	38	1695	38
79	224	81	0.28	0.1034	0.0024	3.718	0.055	0.2621	0.0048	0.0797	0.00225	0.80	1505	28	1575	23	1685	40	1685	40
17	249	152	0.70	0.10326	0.00124	4.1236	0.05532	0.28965	0.00174	0.08396	0.00134	0.45	1640	9	1659	11	1684	21	1684	21
65	439	52	0.12	0.1032	0.0022	3.524	0.055	0.2476	0.0037	0.07208	0.000435	0.66	1426.2	21	1532.4	24	1682	36	1682	36
48	336	184	0.49	0.1031	0.00097	3.9037	0.04138	0.27472	0.00135	0.07892	0.00126	0.46	1565	7	1614	9	1681	17	1681	17
75	241	88	0.34	0.10294	0.0024	3.671	0.06	0.2635	0.00425	0.0777	0.0019	0.77	1508	24	1565	26	1678	39	1678	39
45	365	172	0.17	0.10188	0.00102	3.8882	0.04232	0.27688	0.00119	0.07992	0.00128	0.39	1576	6	1611	9	1659	18	1659	18
88	86	75	0.89	0.1019	0.0023	3.713	0.06	0.2683	0.00425	0.0784	0.0013	0.46	1532	24	1574	25	1658	38	1658	38
24	266	64	0.35	0.10137	0.00116	3.79562	0.05888	0.27157	0.00214	0.07919	0.00061	0.61	1549	11	1592	12	1649	20	1649	20
23	127	73	0.23	0.10114	0.00101	3.9306	0.04753	0.28208	0.00192	0.07951	0.00127	0.56	1602	10	1620	10	1645	17	1645	17
39	445	166	0.08	0.10089	0.00103	3.9361	0.04768	0.28295	0.00175	0.08255	0.00055	0.52	1606	9	1621	10	1641	18	1641	18
84	66	36	0.54	0.0999	0.0025	3.49	0.06	0.2609	0.0047	0.0773	0.00155	0.51	1494	27	1524	26	1620	40	1620	40
72	207	60	0.32	0.0997	0.0026	3.264	0.065	0.239	0.00385	0.06957	0.00065	0.69	1382	22	1475	29	1618	41	1618	41
28	139	72	0.59	0.09927	0.00094	3.7396	0.03869	0.27333	0.00112	0.07997	0.0012	0.4	1558	6	1580	8	1610	17	1610	17
62	197	39	0.21	0.099	0.0021	3.224	0.049	0.2366	0.00365	0.06881	0.00065	0.47	1369	21	1463	22	1605	35	1605	35
31	161	155	0.26	0.09878	0.00112	3.16679	0.04361	0.23252	0.00143	0.06799	0.00043	0.51	1348	7	1449	11	1601	20	1601	20
66	255	82	0.33	0.098	0.0025	3.169	0.06	0.2372	0.0039	0.0699	0.00235	0.81	1372	23	1452	27	1585	40	1585	40
4	132	90	0.63	0.09743	0.00107	2.9738	0.03815	0.22132	0.00146	0.06739	0.00135	0.52	1289	8	1401	10	1576	19	1576	19
21	383	42	0.50	0.09746	0.00136	3.31469	0.05448	0.24667	0.00132	0.07223	0.00037	0.44	1421	7	1485	13	1576	25	1576	25
101	189	85	0.47	0.0972	0.0027	3.21	0.07	0.2409	0.00395	0.0708	0.0011	0.76	1392	23	1459	32	1569	43	1569	43
10	226	68	0.19	0.09683	0.00101	2.55065	0.03123	0.19105	0.00095	0.05598	0.00029	0.46	1127	5	1287	9	1564	19	1564	19
89	87	62	0.73	0.09637	0.0022	3.17	0.05	0.2449	0.0041	0.07135	0.0011	0.38	1412	24	1449	23	1554	36	1554	36
9	127	71	0.28	0.09523	0.00118	3.11122	0.05673	0.23695	0.00237	0.06955	0.00068	0.71	1371	12	1435	14	1533	23	1533	23
38	104	24	0.35	0.09501	0.00135	2.70171	0.06757	0.20623	0.00309	0.06055	0.00088	0.81	1209	17	1329	19	1528	25	1528	25
27	108	51	0.48	0.09378	0.00152	3.36559	0.06968	0.26029	0.00217	0.07652	0.00061	0.56	1491	11	1496	16	1504	29	1504	29
49	519	275	0.38	0.09301	0.00135	3.01686	0.06272	0.23526	0.00238	0.06922	0.00067	0.71	1362	12	1412	16	1488	27	1488	27
59	155	69	0.50	0.0925	0.0023	2.77	0.055	0.2179	0.00335	0.06434	0.00085	0.80	1271	20	1351	27	1475	37	1475	37
41	488	224	0.36	0.09098	0.00109	3.1458	0.04078	0.25081	0.00123	0.0717	0.00122	0.38	1443	6	1444	10	1446	22	1446	22
53	313	139	0.56	0.09046	0.00109	2.9701	0.03896	0.23817	0.00126	0.06857	0.0011	0.4	1377	7	1400	10	1435	22	1435	22
26	195	26	0.44	0.0904	0.00108	3.1056	0.04062	0.2493	0.0013	0.07257	0.00138	0.41	1435	7	1434	10	1434	22	1434	22
92	290	46	0.17	0.08921	0.0019	2.613	0.0365	0.2156	0.00335	0.0675	0.00165	0.66	1258	20	1304	18	1413	30	1413	30
93	170	95	0.59	0.08943	0.0021	2.677	0.043	0.2217	0.00365	0.067	0.0014	0.73	1291	21	1322	21	1413	33	1413	33
90	54	48	0.91	0.08933	0.0022	2.812	0.05	0.2329	0.00385	0.06706	0.00105	0.50	1350	22	1358	24	1410	34	1410	34
3	285	91	0.30	0.08917	0.00088	2.9281	0.03209	0.23824	0.00112	0.06951	0.00111	0.43	1378	6	1389	8	1408	18	1408	18
15	355	59	0.46	0.08917	0.00116	2.9525	0.04134	0.24044	0.00125	0.07117	0.00114	0.37	1389	6	1395	11	1408	24	1408	24
22	195	106	0.53	0.08911	0.00098	2.87	0.04672	0.23344	0.0028	0.07066	0.00113	0.74	1353	15	1374	12	1407	20	1407	20
36	342	62	0.56	0.08895	0.00098	3.01	0.03675	0.24552	0.0013	0.07082	0.00113	0.43	1415	7	1410	9	1403	20	1403	20
32	354	98	0.81	0.08883	0.00089	2.9121	0.03205	0.23799	0.00109	0.06741	0.00108	0.41	1376	6	1385	8	1400	18	1400	18
76	327	87	0.24	0.08872	0.0019	2.762	0.041	0.229	0.00345	0.06961	0.0012	0.41	1329	20	1345	20	1398	30	1398	30
2	151	80	0.49	0.08862	0.00134	2.70704	0.04763	0.22154	0.00122	0.06552	0.00035	0.41	1290	6	1330	13	1396	27	1396	27
74	190	108	0.58	0.0881	0.0020	2.397	0.0375	0.2035	0.00325	0.06042	0.001	0.21	1194	19	1241	19	1393	31	1393	31
78	120	48	0.33	0.0883	0.0025	2.55	0.06	0.219	0.0034	0.0683	0.0029	0.77	1277	20	1297	31	1387	39	1387	39
6	327	113	0.32	0.08755	0.00138	2.12328	0.04346	0.17589	0.00152	0.05209	0.00046	0.64	1044	8	1156	14	1373	30	1373	30
63	173	50	0.30	0.0873	0.0020	2.637	0.047	0.2223	0.00335	0.0653	0.001	0.34	1294	20	1311	23	1365	32	1365	32
16	117	59	0.57	0.08506	0.00166	2.25169	0.05197	0.19199	0.00124	0.05703	0.00034	0.51	1132	7	1197	16	1317	36	1317	36
8	93	38	0.52	0.08413	0.00162	2.49893	0.06433	0.21544	0.00226	0.06407	0.00063	0.64	1258	12	1272	19	1295	37	1295	37
68	284	66	0.25	0.0833	0.0015	2.222	0.026	0.1938	0.0026	0.0573	0.0006	0.87	1142	15	1188	14	1276	23	1276	23
77	293	91	0.26	0.0832	0.0023	2.145	0.0475	0.1889	0.00325	0.0601	0.00375	0.74	1116	19	1167	26	1272	36	1272	36
14	115	43	0.16	0.08303	0.00092	2.04292	0.02954	0.17846	0.00139	0.05315	0.00042	0.6	1059	8	1130	10	1270	20	1270	20
73	167	34	0.22	0.0815	0.0039	1.94	0.085	0.1763	0.00355	0.023	0.0115	0.81	1046	21	1094	48	1220	59	1220	59
103	161	84	0.55	0.0809	0.0023	2.019	0.0445	0.1832	0.00325	0.05471	0.0009	0.80	1084	19	1122	25	1217	34	1217	34
105	415	110	0.27	0.08081	0.0025	2.237	0.055	0.203	0.00365	0.0049	0.0055	0.67	1191	21	1192	29	1216	37	1216	37
43	178	59	0.63	0.08075	0.00089	2.2064	0.02988	0.19828	0.00157	0.06053	0.00097	0.58	1166	8	1183	9	1215	21	1215	21
54	129	78	0.32	0.08041	0.00144	2.16436	0.04548	0.19522	0.0014	0.05834	0.00043	0.47	1150	8	1170	15	1207	34	1207	34
37	128	77	0.22	0.07939	0.00126	1.97095	0.04132	0.18006	0.00188	0.05388	0.00057	0.61	1067	10	1106	14	1182	30	1182	30
29	376	239	0.74	0.07874	0.00087	1.8975	0.02262	0.17482	0.0008	0.0573	0.00092	0.38	1039	4	1080	8	1166	21	1166	21
70	92	57	0.67	0.0784	0.0016	1.862	0.028	0.1775	0.00255	0.0538	0.0011	0.01	1054	15	1071	16	1165	24	1165	24
47	215	81	0.51	0.0784	0.00086	1.4736	0.01793	0.13639	0.00071	0.0564	0.0009	0.43	824	4	920	7	1157	21	1157	4
57	198	195	0.84	0.07807	0.00191	2.08609	0.05827	0.19379	0.00116	0.0581	0.0003	0.41	1142	6	1144	19	1149	48	1149	48
42	117	45	0.31	0.07768	0.00132	1.7741	0.03387	0.16564	0.00088	0.04969	0.00029	0.4	988	5	1036	12	1139	33	1139	33
18	93	70	1.64	0.07672	0.00138	1.5416	0.03069	0.14576	0.00124	0.06016	0.00096	0.43	877	7	947	12	1114	34	1114	7
61	265	75	0.30	0.0764	0.0019	1.742	0.031	0.1649	0.0028	0.04941	0.00075	0.73	984	17	1024	18	1104	27	1104	27
5	389	154	0.37	0.07514	0.00174	1.60026	0.05539	0.15446	0.00242	0.0465	0.0007	0.83	926	14	970	22	1072	46	1072	14
83	314	195	0.61	0.0745	0.0024	1.731	0.0485	0.169	0.0028	0.05078	0.00075	0.68	1007	17	1019	29	1051	34	1051	34
85	412	109	0.26	0.07426	0.0019	1.754	0.0315	0.1726	0.00315	0.0059	0.0015	0.89	1027	19	1028	18	1048	27	1048	27
55	114	39	0.80	0.0742	0.00188	1.80809	0.05348	0.17672	0.00129	0.05328	0.00034	0.43	1049	7	1048	19	1047	50	1047	50
11	488	99	0.28	0.0736	0.00074	1.6949	0.0188	0.16712	0.0008	0.0507	0.00081	0.42	996	4	1007	7	1031	20	1031	20
7	115	104	0.38	0.07341	0.00139	1.66012	0.03485	0.16401	0.00086	0.0495	0.00026	0.33	979	5	993	13	1025	38	1025	38
96	451	110	0.26	0.07242	0.0017	1.61	0.028	0.1614	0.00265	0.0055	0.00195	0.71	964	16	974	17	998	24	998	16
102	525	113	0.23	0.072	0.0030	1.334	0.0475	0.1354	0.00285	0.0387	0.0029	0.94	819	17	859	31	984	41	984	17
56	220	189	0.91	0.07136	0.0021	1.63175	0.05487	0.16583	0.00111	0.05021	0.00028	0.47	989	6	983	21	968	59	968	6
97	109	10	0.09	0.0707	0.0029	1.295	0.046	0.1327	0.0026	0.004	0.013	0.80	803	16	842	30	940	38	940	16
46	247	46	0.35	0.06982	0.00163	1.39587	0.03866	0.145	0.00121	0.04401	0.00042	0.58	873	7	887	16	923	47	923	7
87	322	376	1.18	0.06978	0.0019	1.429	0.03	0.1488	0.0025	0.0342	0.0015	0.68	894	15	901	19	922	25	922	15
44	247	167	0.44	0.06859	0.00138	1.44311	0.03522	0.1526	0.0012	0.04641	0.00035	0.56	916	7	907	15	886	41	916	7
107	541	131	0.24	0.06755	0.0024	1.289	0.036	0.1382	0.003	0.011	0.0013	1.00	834	18	840	23	854	30	834	18
100	367	40	0.11	0.06422	0.0026	1.077	0.039	0.1214	0.00235	-0.0116	0.00275	0.93	738	14	745	27	749	31	738	14
104	1076	164	0.16	0.06415	0.0017	1.059	0.0215	0.1197	0.00195	-0.01	0.0013	1.00	728.6	12	733	15	747	19	729	12
71	342	62	0.20	0.06357	0.0013	0.999	0.012	0.1141	0.0018	0.004	0.00215	1.00	696.5	11	703.4	8	727	14	697	11
80	503	148	0.23	0.06312	0.0015	0.979	0.0165	0.1125	0.00185	0.0017	0.0011	1.00	687	11	693	12	712	17	687	11
35	201	58	0.17	0.06523	0.00153	0.92247	0.02476	0.10256	0.00083	0.03137	0.00047	0.53	629	5	664	13	782	47	629	5
91	183	130	0.75	0.0603	0.0012	0.802	0.008	0.0965	0.0017	0.0634	0.0017	1.00	593.7	10	598	6	614	12	594	10
20	389	136	0.10	0.0578	0.00115	0.66494	0.01461	0.08343	0.00057	0.02588	0.00038	0.43	517	3	518	9	522	42	517	3
95	377	89	0.25	0.0551	0.0024	0.611	0.0245	0.0803	0.00135	0.0451	0.00225	0.55	498.1	8	483	19	400	17	498	8
94	236	36	0.16	0.0591	0.0023	0.641	0.0185	0.08	0.00205	0.0155	0.0045	0.96	496	13	502	14	567	22	496	13
69	166	29	0.19	0.0547	0.0019	0.568	0.0165	0.0753	0.00135	0.0229	0.00105	0.28	467.9	8	456	13	393	13	468	8